Geochemistry, Geophysics, Geosystems

RESEARCH ARTICLE
10.1029/2019GC008402

Pacific-Panthalassic Reconstructions: Overview, Errata and the Way Forward

Trond H. Torsvik[1,2], Bernhard Steinberger[3,1], Grace E. Shephard[1], Pavel V. Doubrovine[1], Carmen Gaina[1], Mathew Domeier[1], Clinton P. Conrad[1], and William W. Sager[4]

[1]Centre for Earth Evolution and Dynamics (CEED), University of Oslo, Oslo, Norway, [2]School of Geosciences, University of Witwatersrand, Johannesburg, South Africa, [3]Helmholtz Centre Potsdam, GFZ, Potsdam, Germany, [4]Department of Earth and Atmospheric Sciences, University of Houston, Houston, TX, USA

Key Points:
- We devised a new absolute Late Jurassic-Cretaceous Pacific plate model
- This study was motivated because published Pacific plate models (83.5–150 Ma) are variably flawed
- The emplacement of the Shatsky Rise Large Igneous Province at ~144 Ma caused a major plate boundary reorganization

Correspondence to:
T. H. Torsvik,
t.h.torsvik@geo.uio.no

Citation:
Torsvik, T. H., Steinberger, B., Shephard, G. E., Doubrovine, P. V., Gaina, C., Domeier, M., et al. (2019). Pacific-Panthalassic reconstructions: Overview, errata and the way forward. *Geochemistry, Geophysics, Geosystems*, *20*, 3659–3689. https://doi.org/10.1029/2019GC008402

Received 24 APR 2019
Accepted 26 JUN 2019
Accepted article online 4 JUL 2019
Published online 29 JUL 2019

Abstract We have devised a new absolute Late Jurassic-Cretaceous Pacific plate model using a fixed hot spot approach coupled with paleomagnetic data from Pacific large igneous provinces (LIPs) while simultaneously minimizing plate velocity and net lithosphere rotation (NR). This study was motivated because published Pacific plate models for the 83.5- to 150-Ma time interval are variably flawed, and their use affects modeling of the entire Pacific-Panthalassic Ocean and interpretation of its margin evolution. These flaws could be corrected, but the revised models would imply unrealistically high plate velocities and NR. We have developed three new Pacific realm models with varying degrees of complexity, but we focus on the one that we consider most realistic. This model reproduces many of the Pacific volcanic paths, modeled paleomagnetic latitudes fit well with direct observations, plate velocities and NR resulting from the model are low, and all reconstructed Pacific LIPs align along the surface-projected margin of the Pacific large low shear wave velocity province. The emplacement of the Shatsky Rise LIP at ~144 Ma probably caused a major plate boundary reorganization as indicated by a major jump of the Pacific-Izanagi-Farallon triple junction and a noteworthy change of the Pacific-Izanagi seafloor spreading direction at around chron M20 time.

1. Introduction

The Pacific plate is the largest tectonic plate on Earth and hosts many hot spots, a vast number of volcanic seamounts, and large Cretaceous volcanic areas known as Large Igneous Provinces (LIPs; Coffin & Eldholm, 1994; Eldholm & Coffin, 2000; Bryan et al., 2010; Ernst, 2014). These include the Shatsky, Hess, and Magellan rises, the Ontong Java, Manihiki and Hikurangi plateaus, the Nauru Basin, and the Mid-Pacific Mountains (Figure 1). The Pacific plate also features the prominent Hawaiian-Emperor volcanic chain stretching almost 6,000 km from the active submarine volcano Lōʻihi near Hawaii to the Detroit (81–75 Myrs old) and Meiji (>82 Myrs old) seamounts in the northwest Pacific (Figure 1). The cause for the eye-catching 60° bend that formed at ~47 Ma has been debated for decades and interpreted as the result of an abrupt Pacific plate motion change, a rapid southward drift of the Hawaiian hot spot before the formation of the bend, or a combination of these two end-member explanations (e.g., Torsvik et al., 2017 and section 3).

Reconstructing the history of the Pacific Ocean and its predecessor—the Panthalassic Ocean—is a challenging endeavor. This is in part due to the loss of lithosphere by subduction processes, as more than 95% of the Panthalassic-Pacific lithosphere has been subducted since the Late Jurassic (150 Ma). Cretaceous seafloor spreading within the Pacific-Panthalassic domain is classically modeled as a system of four main plates (Figure 2a), the Pacific and the surrounding Izanagi, Farallon, and Phoenix plates which are thought to have existed for most of the Mesozoic (e.g., Matthews et al., 2016; Müller et al., 2016; Seton et al., 2012; Shephard et al., 2013). However, their oceanic lithosphere has been near entirely lost to subduction, and hence, the configuration of their boundaries is largely derived from kinematic models linked to the absolute motion of the Pacific plate.

The Ontong Java, Manihiki, and Hikurangi LIPs (Figure 1) are commonly considered as being formed as one single vast LIP—the Ontong Java Nui (Taylor, 2006)–which erupted at ~123 Ma and led to the breakup of the Phoenix Plate into four new plates (Chandler et al., 2012), Hikurangi, Manihiki, Chazca, and Catequil plates

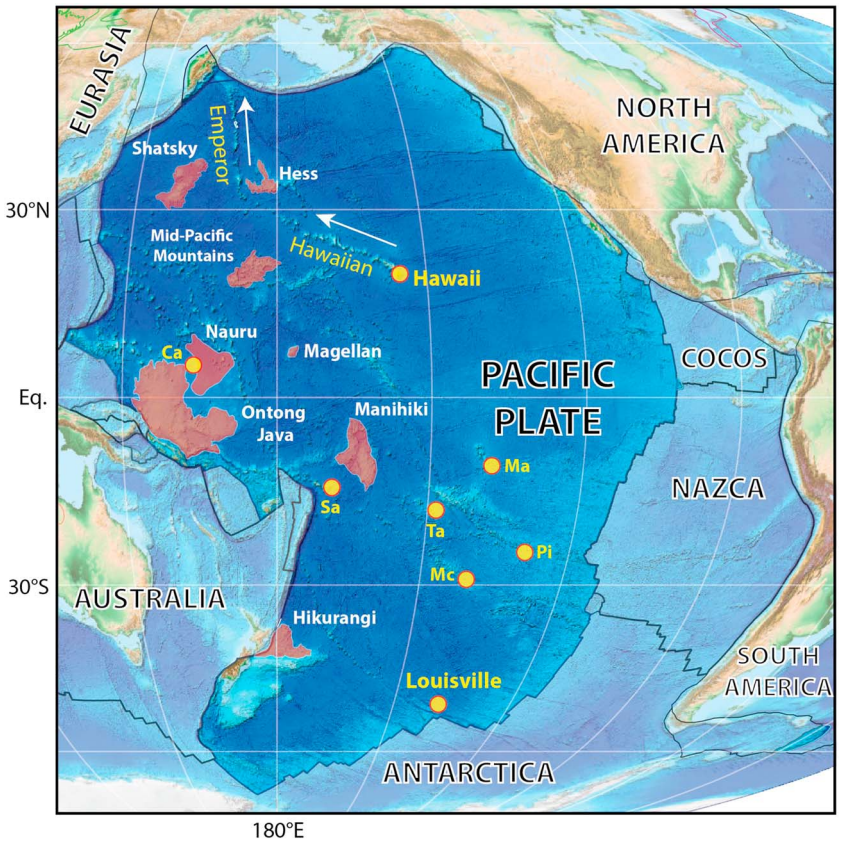

Figure 1. The modern Pacific region and the location of large igneous provinces (transparent red shading: Shatsky Rise, Hess Rise, Mid-Pacific Mountains, Ontong Java Plateau, Magellan Rise, Manihiki Plateau, Hikurangi Plateau, and Nauru Basin) and hot spots (yellow-shaded circles) on the Pacific plate inferred to be sourced by deep-rooted plumes (French & Romanowicz, 2015). These hot spots are Ca, Caroline; Hawaii; Louisville; Ma, Marquesas; Mc, Macdonald; Pi, Pitcairn; Sa, Samoa; Ta, Tahiti. The Pacific plate is the largest tectonic plate on our planet—covering more than 20% of the Earth's surface—and is moving in a northwesterly direction that parallel's the Hawaiian Chain (white arrow). Before 47 Ma it moved northward (white arrow) and paralleled the Emperor Chain (47–80 Ma), according to Torsvik et al. (2017).

(Figure 2b). After an inferred Pacific reorganization at ~85 Ma (Figure 2c), when Manihiki, Hikurangi, and parts of Catequil (other portions and Chazca relocated to Farallon) became part of the Pacific plate (e.g., Matthews et al., 2016), the Pacific plate became the dominant tectonic plate in the Pacific Ocean, and from that time we refer to the ocean basin as the Pacific Ocean.

The Pacific-Panthalassic oceans were the largest Mesozoic-Cenozoic oceans on Earth, and their margins constituted the main subduction factories. The plate motion history for the Pacific plate is therefore critical for building robust global plate kinematic and geodynamic models. In this paper, we revisit the absolute plate motion of the Pacific plate by critically assessing existing models (for the last 150 Ma) and then present a new solution that reflects our present knowledge of this plate, with a focus on intraplate volcanism, records of marine magnetic anomalies, and paleomagnetic data.

2. Absolute Plate Motion Frames

Tectonic plates can be reconstructed in an absolute sense (e.g., relative to the mantle) using the geometry and ages of hot spot volcanoes. Many hot spot frames have been developed since the first one was constructed in the early 1970s (Morgan, 1972a, 1972b), but these typically assumed hot spot fixity and were defined separately for the Pacific (e.g., Duncan & Clague, 1985) and Indo-Atlantic domains (e.g., Müller et al., 1993). The recognition of hot spot mobility (e.g., Molnar & Stock, 1987; Steinberger, 2000; Steinberger & O'Connell, 1998; Tarduno & Cottrell, 1997) led to the emergence of a new generation of hot

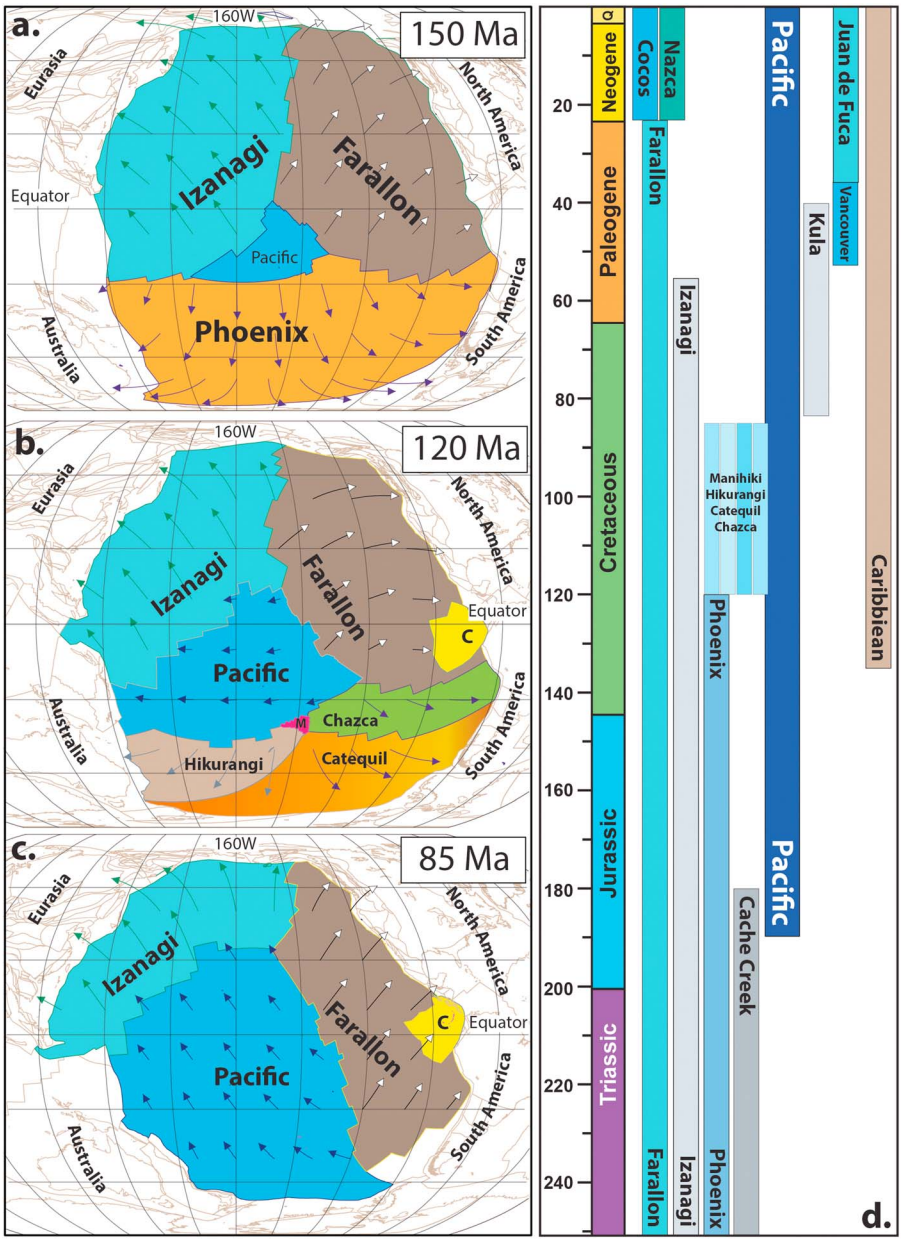

Figure 2. Panthalassic-Pacific reconstructions at (a) 150, (b) 120, and (c) 85 Ma with plate velocity vectors with respect to a mantle frame. Matthews et al. (2016) model, but with a new absolute mantle frame for the Pacific (Model S, this study), and adjusted dynamic polygon model. C, Caribbean Plate; M, Manihiki Plate. (d) Important Mesozoic to modern Panthalassic-Pacific plates and their life span according to the Matthews et al. (2016) model and references therein. In this model, the Phoenix Plate essentially split into four plates (Manihiki, Hikurangi, Catequil, and Chazca) at around 120 Ma, which later became part of the Pacific (Manihiki, Hikurangi, and parts of Catequil) and the Farallon (Chazca) plates at around 85 Ma. Kula formed from pieces of the Pacific, Izanagi, and Farallon plates at around 83 Ma and became part of the Pacific plate at around 40 Ma. The Farallon Plate split into the Nazca and Cocos plates around 23 Ma.

spot frames, in which motions of hot spots were modeled numerically and attempts were made to fit hot spot tracks globally, linking them through circuits of relative plate motion. These are referred to as "global moving hot spot reference frames" (GMHRF), the first one being developed by Steinberger et al. (2004), and here called GMHRF-1. This model, which extended back to 83.5 Ma, yielded reasonable fits to the geometries and age progressions of four hot spot tracks linked to the Hawaiian and Louisville hot spots (in the Pacific), and to the Tristan and Reunion (back to 66 Ma) hot spots in the Atlantic and Indian

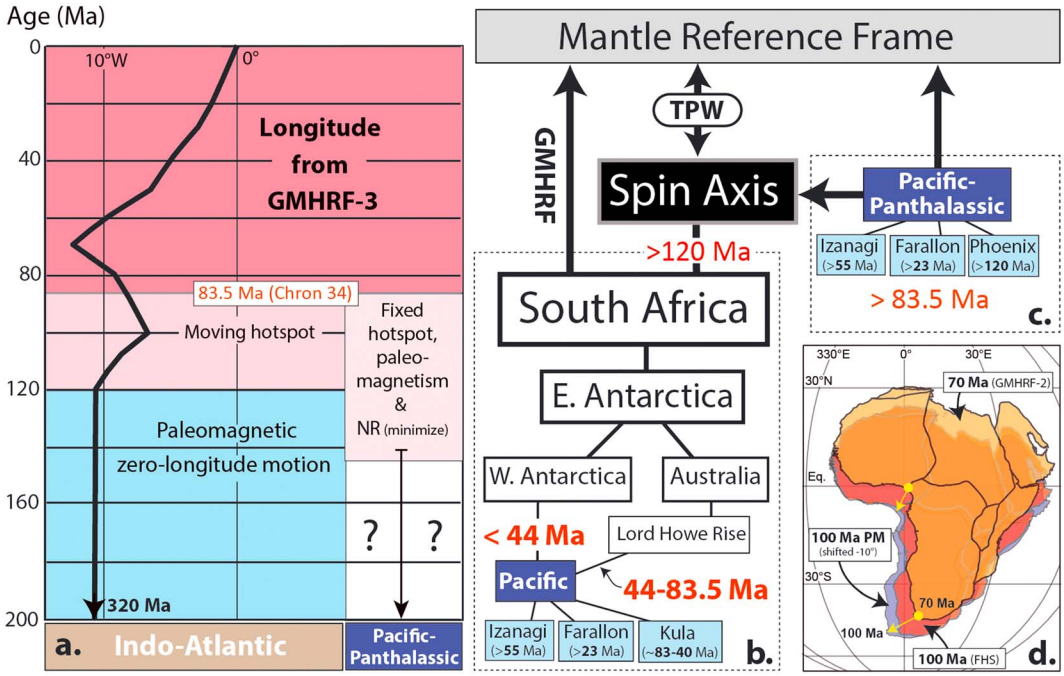

Figure 3. (a) Longitude motion of the African plate over the past 200 Ma (solid black line; Doubrovine et al., 2016). This is a hybrid mantle reference frame using global moving hot spot reference frames (GMHRF-3) to 83.5 Ma, then a moving hot spot frame for the Indo-Atlantic to 120 Ma (Doubrovine et al., 2012), and finally a true polar wander- (TPW-)corrected longitude-calibrated (shifted 10.6°W) paleomagnetic frame before that time (Torsvik et al., 2012). Here shown to 200 Ma but extendable to about 320 Ma (Pangea assembly). The Pacific-Panthalassic plates are part of the GMHRF to 83.5 Ma, and before that time, we use a fixed hot spot frame combined with TPW-corrected paleomagnetic data (this study). (b) Example of a hierarchical reconstruction network. All plates (here only shown for linking the Pacific to the Indo-Atlantic) are first referenced to South Africa (the anchor plate) through relative motions. The entire relative motion network is then restored to an absolute framework by the reconstruction of South Africa according to hot spot track data or paleomagnetic data (before 120 Ma in our model). Note that two relative plate circuit models (Steinberger et al., 2004) have been used for reconstructing relative motions between the Pacific plate and plates of the Indo-Atlantic hemisphere (white boxes). Before ~44 Ma (chron 20) the Pacific plate follows a plate motion chain through Australia and Lord Howe Rise, and after that time a plate motion chain through East Antarctica and West Antarctica (Marie Byrd Land). (c) GMHRFs (Doubrovine et al., 2012; Steinberger et al., 2004; Torsvik et al., 2008) in panel (b) are only truly *global* for the past 83.5 Ma because the Panthalassic-Pacific plates are reconstructed independently before that time because there are no known plate circuits to link the Pacific and Indo-Atlantic realms. The Pacific plate can theoretically be reconstructed to 144 Ma (Shatsky Rise LIP) in a fixed hot spot scheme (but often extrapolated to 150 Ma). Other plates in the Pacific are mostly networked to the Pacific plate; before 144 Ma Panthalassic-Pacific reconstructions are not constrained in terms of absolute plate motions. (d) Müller et al. (2016) used a modification of GMHRF-2 (Torsvik et al., 2012) to reconstruct Africa, but only back to 70 Ma, since they argued that hot spot reference frames are unreliable before that time. From 100 Ma they used a TPW-corrected paleomagnetic frame (Torsvik et al., 2012) that was adjusted somewhat arbitrarily −10° in longitude, and between 70 and 100 Ma they merged the two frames by linear interpolation (yellow arrows). Here we reconstruct Africa at 100 Ma with the paleomagnetic (PM) frame adjusted −10° in longitude to show that the fixed hot spot reconstruction in GMHRF-2 at 100 Ma matches very well the paleomagnetic one except for a minor angular and longitude discordance. Deeming hot spot reference frames unreliable before 70 Ma (Müller et al., 2016) is therefore *not* justifiable. Net TPW is approximately zero at 100 Ma (Torsvik et al., 2012).

Oceans, respectively. GMHRF-2 (Torsvik et al., 2008) used the same plate motion hierarchy, but was extended from 83.5 to 130 Ma for the Indo-Atlantic domain, and to 150 Ma for the Pacific hemisphere, using rotation rates relative to fixed hot spots. But importantly, the extension from 83.5 to 130 Ma was undertaken separately for Africa/Indo-Atlantic (Figure 3b) and the Pacific (Figure 3c). GMHRF-3 (Doubrovine et al., 2012) included a fifth hot spot track, the New England Seamount Chain (Central Atlantic), a revision of the Reunion track (Torsvik et al., 2013) and incorporated a separate extension for the African (using rotation rates relative to moving hot spots) and Pacific plates from 83.5 to 120 Ma that differed from GMHRF-2 (Table 1).

Reconstructions of tectonic plates relative to Earth's spin axis are achieved by using paleomagnetic data that can be used to constrain the paleolatitude and azimuthal orientation of lithospheric blocks, but this method cannot constrain past longitudes. Therefore, the absolute longitudinal position of plates for ages older than the Cretaceous (oldest hot spot tracks) is unknown. To circumvent this shortcoming of the paleomagnetic method, one can estimate the paleolongitude of a plate that is thought to have moved the least since Pangea assembly (~320 Ma), and whose subsequent relative motion can be easily retraced. This plate can

Table 1
Details and Explanations for Some Selected Mantle Reference Frames Discussed in the Text

Reference	Global 0–83.5 Ma	Indo-Atlantic	Pacific extension
		Extended beyond 83.5 Ma	
Steinberger et al. (2004)	GMHRF-1: Moving hot spots (4 tracks)	None	
Steinberger and Gaina (2007)	None		ERRATA: Fixed hot spot based on Duncan and Clague (1985)
Torsvik et al. (2008)	GMHRF-2: Moving hot spots (4 tracks)	Fixed hot spots (2 tracks) + TPW-corrected data (Steinberger & Torsvik, 2008) before 100 Ma	As in Steinberger and Gaina (2007)
Torsvik et al. (2010)	Note: Differ from all other frames because the Pacific (based on Steinberger & Gaina, 2007) and Indo-Atlantic frames have been computed separately (O'Neill et al., 2005; smooth version; see also Torsvik et al., 2008): We thus infer plate circuits between the Pacific and Indo-Atlantic realms from the two independent reference frames		As in Steinberger and Gaina (2007)
Doubrovine et al. (2012)	GMHRF-3: Moving hot spots (5 tracks)	Moving hot spots (2 tracks) back to 124 Ma	Fixed hot spot based on (i) Duncan and Clague (1985), or (ii) Wessel and Kroenke (2008, WK08-A) back to 120 Ma
Matthews et al. (2016) (similar but not identical to Müller et al., 2016)	GMHRF-2 until 70 Ma but different plate circuits (including Pacific to the Indo-Atlantic)	Crossbreed of GMHRF-2 (until 70 Ma) and TPW-corrected data (Torsvik et al., 2012) from 100 Ma and backward. Interpolated from 70 to 100 Ma; plate circuits changed.	Errata 2 Fixed hot spot based on Wessel and Kroenke (2008, WK08-A), but the authors computed stage rotations from this model by multiplying finite rotation matrices FROT at times $t1$ and $t2$ in the wrong order (symbolically $[FROT^{t2} - FROT^{t1}]$ instead of $[-FROT^{t1} + FROT^{t2}]$ as explained in Cox & Hart, 1986)

Note. GMHRF, Global Moving Hot spot Reference Frame.

then be established as the *root* of the global relative plate motion model, which can be further cast into an absolute reference frame. An assumption of "zero-longitude" motion for Africa was therefore proposed by Burke and Torsvik (2004) and used to develop hybrid mantle frames combining hot spot- and paleomagnetic-based reconstructions (Doubrovine et al., 2012, 2016; Torsvik et al., 2008, 2010). The first use of this method kept Africa strictly fixed in longitude back to 200 Ma (Burke & Torsvik, 2004), but it is known from hot spot reference frames that Africa did move somewhat in longitude, between ~5° (O'Neill et al., 2005; Torsvik et al., 2008) and ~11° (Doubrovine et al., 2012) since the Late Cretaceous. To build a hybrid reference frame, we first employ a hot spot reference frame back to a certain time at which hot spot tracks become insufficient (poorly constrained) or altogether absent (e.g., 120 Myr in Doubrovine et al., 2012). For earlier times, we switch to paleomagnetic reconstructions but apply a longitude correction according to the longitude difference between the hot spot and paleomagnetic reference frames at the transition time. The paleomagnetic reconstructions must also be corrected for true polar wander (TPW), because they are constructed relative to the Earth's spin axis and not relative to the mantle, as in the hot spot reference frames. TPW affects the entire planet, including the oceanic domains, and therefore the Pacific-Panthalassic plates must obey the same TPW rotation as the continental plates. For example, Torsvik et al. (2012) determined TPW episodes between 150 and 140 Ma (Figure 4), and between 110 and 100 Ma, around an equatorial axis piercing the surface at 11°E and its antipode at 169°W.

Global reference frames that combine hot spot and TPW-corrected paleomagnetic reconstructions are known as a global hybrid mantle reference frame (Steinberger & Torsvik, 2008; Torsvik et al., 2008), and the one we prefer is detailed in Doubrovine et al. (2016) and Torsvik and Cocks (2017). The default rotation file distributed by GPlates application versions 2.0/2.1 (www.gplates.org) also uses a global hybrid mantle reference frame, but the plate motion model (Matthews et al., 2016) adopted a modified version of GMHRF-2 (Torsvik et al., 2008) for the past 70 Myr and is directly connected to an Indo-Atlantic TPW-corrected paleomagnetic frame at 100 Ma (Torsvik et al., 2012) with a longitude correction of -10^{o}

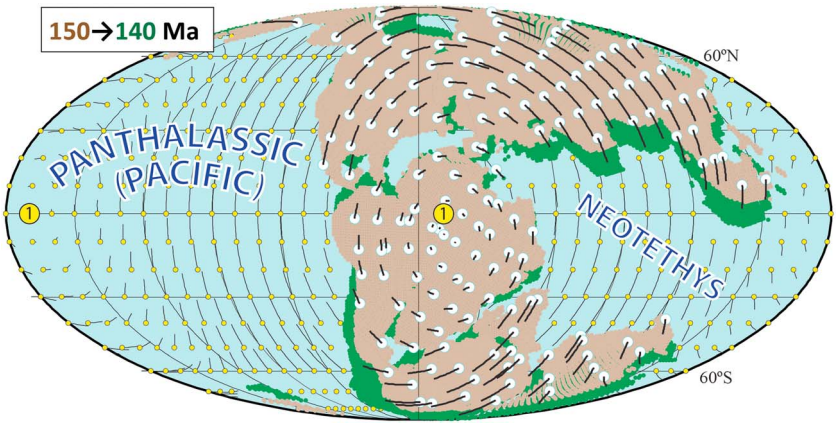

Figure 4. True polar wander (TPW) is observed between 150 and 140 Ma at a rate of 0.8°/Ma (Torsvik et al., 2012), and total motions are shown as black lines connected to white dots with the sense of motion from the white dot toward the tail. Open yellow circles are the center for TPW (0°N, 11°E or its antipode at 169°W). Light brown (green) shading represents the continental reconstruction at the start (end) of the TPW episode. TPW affects the entire planet and the oceanic domains (e.g., Panthalassic-Pacific and Neotethys) must experience the same TPW rotation (thinner black lines).

(Müller et al., 2016). The 70- to 100-Ma interval in between is linearly interpolated and thus smoothed. Müller et al. (2016) selected a 70-Ma transition time because they considered the hot spot reference frame in Torsvik et al. (2008) to be unreliable before that time. Note, however, that GMHRF-2 yields a 100-Ma hot spot reconstruction that is virtually identical to the longitude-calibrated (−10°) paleomagnetic reconstruction (Figure 3d).

The Pacific plate can be directly linked through regional plate circuits to the Indo-Atlantic realm only for the last 83.5 Ma (Figure 3a), but debates continue about the best relative motion pathway (Steinberger et al., 2004; Torsvik et al., 2017; Wright et al., 2015). Before 83.5 Ma, the Pacific plate was surrounded by subduction zones that cannot be directly connected with the rest of the relative motion chain. It follows that the motion of the Pacific plate must be referenced directly to the mantle using fixed hot spot schemes (Figure 3c). However, such schemes only work back to ~150 Ma, and before that time, there are no means of reconstructing the Panthalassic plates in an absolute sense relative to the mantle. In principle, motion of hot spots could also be considered back to 150 Ma. However, mantle flow and hence hot spot motion becomes increasingly uncertain further back in time, therefore we regard fixed hot spots as the most suitable approximation for times earlier than 83.5 Ma.

3. Pacific Plate Motion Inferred From Hot Spot Tracks (0–83.5 Ma)

The Hawaiian-Emperor and Louisville volcanic chain tracks can be used to determine the motion of the Pacific plate independently relative to the mantle (e.g., Steinberger & Gaina, 2007; Torsvik et al., 2008, 2010, Table 1). But these two volcanic chains are also incorporated in the construction of the GMHRF that uses relative plate circuits to link the Pacific realm to the Indo-Atlantic realm. An example of how GMHRF-3 reproduces the Hawaiian-Emperor Chain is shown in Figure 5a. This model fits the observed seamount locations and ages within model uncertainties. Torsvik et al. (2017) have also demonstrated that the trends of the Hawaiian and Emperor seamounts can be reproduced in this model even without the motion of the Hawaiian hot spot relative to the mantle, so that the entire 60° bend is explained by a change in the Pacific plate motion at around 47 Ma (Figure 5b). However, southward drift of the Hawaiian mantle plume is required to explain about 800 km out of the total length (2,000 km) of the Emperor Chain. This is shown by a simple sketch (Figure 5c), where the Pacific plate motion path changes at around 47 Ma, but the 80- to 47-Ma segment of the motion path (red thick line) is ~800 km shorter compared with the length of the Emperor Chain (yellow line in Figure 5c). This difference is the effect of southward hot spot drift for the past 80 Myr in GMHRF-3 (blue line in Figure 5c). Similarly, the Pacific plate motion path also changes at 47 Ma in GMHRF-2 (compare red and green lines in Figure 5b), but the modeled southward hot spot drift is larger in this GMHRF and the Emperor Chain is lengthened by ~1,200 km. Both models suggest a *straightforward*

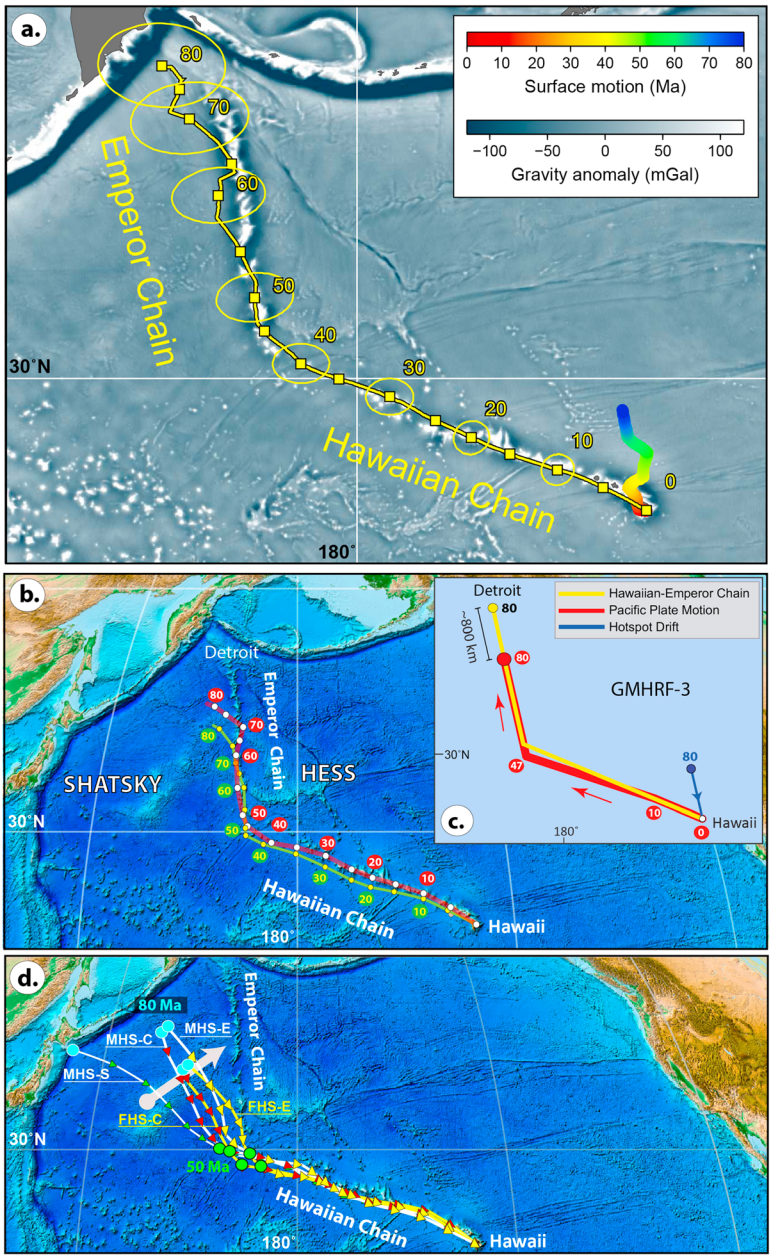

Figure 5. (a) Model hot spot track (yellow line; yellow squares with uncertainty ellipses at 10-Myr intervals) computed by combining the motion of the Pacific Plate in global moving hot spot reference frames (GMHRF-3; Doubrovine et al., 2012) and the geodynamically modeled surface motion of the Hawaiian hot spot (rainbow-colored swath; also from Doubrovine et al., 2012). (b) The red line (5 Myr intervals) shows the track that would be produced if the Hawaiian hot spot were fixed in GMHRF-3, that is, reflects the Pacific Plate motion alone (see Torsvik et al., 2017; Torsvik & Cocks, 2017). The Pacific motion path is compared with the predicted GMHRF-2 (Torsvik et al., 2008) Pacific motion path (green line, yellow circles). (c) Cartoon explaining GMHRF-3 where the yellow line is the idealized track of the Hawaiian-Emperor Chain (as in panel a) and the red line is Pacific plate motion path that changes at 47 Ma but is displaced southward compared with the Hawaiian-Emperor Chain: That is the effect of southward hot spot drift for the past 80 Myrs (blue line), which has lengthened the Emperor Chain by ~800 km. A similar explanation applies to the older GMHRF-2 but in this model the southward hot spot drift is larger and has lengthened the Emperor Chain by ~1,200 km. (d) The prediction of the Hawaiian hot spot track from Indo-Atlantic ("African") hot spots based on fixed hot spot (FHS, yellow lines: Müller et al., 1993 revised in Torsvik et al., 2008) and moving hot spot (MHS, white lines: O'Neill et al., 2005) frames. The predicted tracks are shown in 5-Myr intervals from 80 Ma and calculated with two different plate circuits linking the Pacific to Africa: FHS-C and MHS-C based on the model we use (Figure 3b; based on Steinberger et al., 2004), while FHS-E and MHS-E follows Matthews et al. (2016) where the Pacific plate is linked via Marie Byrd Land/West Antarctica (Wright et al., 2015), and then through East Antarctica to Africa. The predicted tracks plot west of the Emperor Chain but all indicate a plate motion change at around 50 Ma. Conversely, older plate circuit models did not predict the Hawaiian-Emperor bend (HEB): This is exemplified with plate motion model A of Steinberger et al. (2004; white line with green triangles and marked MHS-S) in an Indo-Atlantic moving hot spot frame (O'Neill et al., 2005). Appropriate plate circuits are critical to predict the HEB from Indo-Atlantic hot spots as illustrated by the large gray arrow that indicates the improved prediction of the HEB with new plate circuits linking the Pacific Plate and Africa over the past three decades.

history of the Pacific plate motion since 83.5 Ma: the Pacific plate moved in a northward direction (near parallel to the Emperor Chain) between 80 and 47 Ma and then changed to a northwesterly direction parallel to the Hawaiian Chain (Figure 5c).

Initial concerns on fixed hot spot reference frames (e.g., Molnar & Stock, 1987) emerged from the observation that the expected Hawaiian hot spot track from the Indo-Atlantic hot spots did not predict the HEB but rather indicated a general northwestward movement of the Pacific Plate for the past 80 Myrs (e.g., white curve marked MHS-S in Figure 5d). This critically depends on the plate circuits linking the Pacific Plate to Africa as demonstrated in Steinberger et al. (2004). Based on refinements of their model B (Doubrovine et al., 2012; Figure 3b), HEB is clearly predicted from both fixed and moving Indo-Atlantic hot spot frames (curves marked MHS-C and FHS-C in Figure 5d). New plate circuits between the Pacific Plate and Marie Byrd Land/West Antarctica (Wright et al., 2015), but more importantly revised plate circuits between West and East Antarctica (Granot et al., 2013 model extended beyond ~40 Ma)—as implemented in Matthews et al. (2016)—predicts the HEB even more pronouncedly (curves marked MHS-E and FHS-E in Figure 5d). The HEB is therefore clearly predicted by a plate motion change from Indo-Atlantic hot spots in both fixed and moving hot spot reference frames, and with two different plate circuit models. Before 50 Ma all the predicted curves are located to the west of the Emperor Chain (depending on the relative plate circuits linking the Pacific plate to Africa), but they are also shorter than the Emperor Chain, notably in a fixed Indo-Atlantic hot spot frame (curves FHS-C & FHS-E in Figure 5d), because the Emperor Chain is lengthened by the southward drift of the Hawaiian hot spot (Figure 5c).

4. Pacific Plate Motion Relative to Hot Spots (or Mantle) Before 83.5 Ma: A Scrutiny of Previously Published Models

In the absence of a direct kinematic link between the Pacific plate and the rest of the global plate circuit, the only way to describe and incorporate its motion is to inspect the volcanic features of this plate that recorded its motion relative to a quasi-stationary mantle anomaly (hot spot). Duncan and Clague (1985) and Wessel and Kroenke (2008) developed pre-83.5-Ma absolute plate motion models based on the geometry and ages of Pacific seamount chains, and the assumption that the seamounts were sourced by fixed hot spots. The Duncan and Clague (1985) model is very smooth, based on old geochronology data from few, diffuse seamount chains, and a single stage pole describes the Pacific plate motion between 100 and 150 Ma. Wessel and Kroenke (2008) developed a more sophisticated, high-resolution model with uncertainty estimates back to ~145 Ma (Figure 6a). The modeled Pacific plate hot spot tracks for the two models are quite different. For example, assuming the Shatsky and Hess rises as a part of an extant hot spot track, and an initial plume location beneath the southern Shatsky Rise, the Duncan and Clague (1985) model predicts a direct connection between the Shatsky (144 Ma) and Hess (~100 Ma) rises, whereas the Wessel and Kroenke (2008) model shows a more complex trajectory reflecting its higher temporal resolution (Figure 6c).

Torsvik et al. (2010), following Steinberger and Gaina (2007), added stage poles derived from Duncan and Clague (1985) to their Late Mesozoic-Cenozoic model, while public releases of GPlates (e.g., GPlates 2.0/2.1 based on Matthews et al., 2016) used smoothed stage poles based on Wessel and Kroenke (2008, WK08-A model). A close inspection of these models shows that the pre-83.5-Ma rotations for the Pacific plate are incorrect in Steinberger and Gaina (2007). This is also the case for subsequent models like Seton et al. (2012), Shephard et al. (2013), Müller et al. (2016), Matthews et al. (2016), and regrettably all public releases of GPlates-associated global plate models (hereafter also referred to as the *Earthbyte* model). Here we describe why these models are flawed and present the corrected rotations (Tables 2 and 3). Because of the time period concerned, the errors we have identified are not related to the plate circuit connecting Africa to the Pacific. We also propose new models for the Pacific plate between 83.5 and 150 Ma (Tables 4 and 5), which are also made available in GPlates format (Appendix A).

4.1. Erratum 1

Torsvik et al. (2010) published the first global full-plate model that used a beta version of the GPlates dynamic polygon functionality (Gurnis et al., 2012); the model also incorporated estimates of predrift extension, but was used primarily to estimate net lithosphere rotation (NR) for the past 150 Myr. Torsvik et al. (2010) and others (e.g., Conrad et al., 2013) used a Pacific plate model that was extended from 83.5 Ma (Steinberger & Gaina, 2007) with stage-poles from Duncan and Clague (1985). However, the Euler

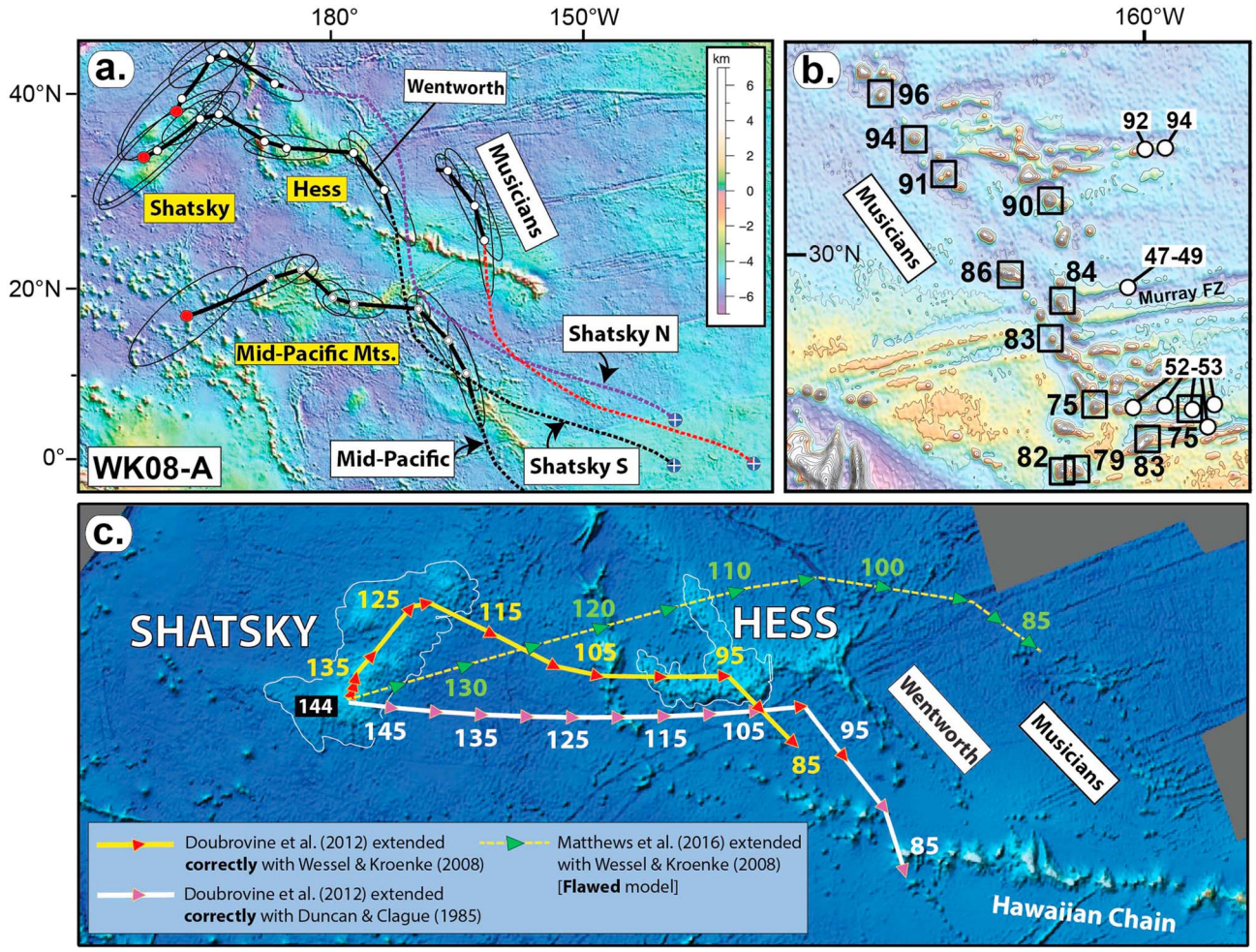

Figure 6. (a) Predicted Pacific plate tracks and 95% confidence ellipses of the WK08-A model for Shatsky North (N) and South (S), the Musicians seamount chain, and the Mid-Pacific Mountains (after Wessel & Kroenke, 2008). (b) Compilation of ages from the Musicians seamounts, which suggests a rather clear-cut age progression from north to south (96–75 Ma; see Clouard & Bonneville, 2005) but is complicated by the fact that recent isotope ages from the southern Musician ridges (open white circles) yield $^{40}Ar/^{39}Ar$ ages between 52–53 Ma and 47–49 Ma (O'Connor et al., 2015). (c) Doubrovine et al. (2012) GMHRF-3 extended (correctly) back to 144 Ma with stages poles after Duncan and Clague (1985) and Wessel and Kroenke (2008). The Pacific plate tracks here assume an initial plume center below south Shatsky Rise. We also show the predicted track from the flawed *Earthbyte* model (Matthews et al., 2016; stippled yellow line), which should have mimicked the Wessel and Kroenke (2008) track (thick yellow line) but is plainly different and does not at all link the Shatsky and Hess Rises because of erroneous stage pole calculations (see Table 1 and text).

rotation poles in Table IV of Duncan and Clague (1985) were interpreted as stage poles of the Pacific plate over fixed hot spots, whereas they actually represent inverted stage poles of the Pacific fixed hot spot frame relative to the Pacific plate. Table DR1 in Steinberger and Gaina (2007)—adopted in, for example, Torsvik et al. (2010)—is therefore incorrect and rectified finite rotations (90 to 150 Ma) are listed in Table 2. The revised rotations (Figures 7a and 8a) do not significantly affect the absolute speed of the Pacific plate, but because most plates in the Pacific Ocean are directly linked through seafloor spreading with that plate, changes in the orientation of the Pacific plate significantly affect the relative motions of other adjacent plates, and therefore the NR as the entire Pacific basin is "rotating" in the corrected model. Figure 8a shows the difference between the flawed and corrected reconstructions, the difference in the orientation of the Pacific plate only amounts to a maximum of 9° at 150 Ma (Figure 7a) but leads to a ~25% increase in NR between 120 and 110 Ma (Table 2).

4.2. Erratum 2

The plate motion model of Matthews et al. (2016) uses a modified version of GMHRF-2 (Torsvik et al., 2008) for the past 70 Myrs that is connected to an Indo-Atlantic TPW-corrected paleomagnetic frame at 100 Ma

Table 2
Absolute Motions for the Pacific Plate and Net Lithosphere Rotation (NR; Torsvik et al., 2010) Based on a Moving Hot Spot Frame After 83.5 Ma and a Fixed Hot Spot Frame Back to 150 Ma (Steinberger & Gaina, 2007; Duncan & Clague, 1985)

Age	Pacific (Torsvik et al., 2010)				Pacific corrected			
(Ma)	Lat.	Long.	Angle	NR	Lat.	Long.	Angle	NR
10	72.6	−63.7	8.5	0.14				
20	72.6	−63.7	17.0	0.15				
30	71.1	−62.1	23.4	0.10				
40	68.7	−60.1	27.7	0.10				
50	65.0	−63.4	31.4	0.08				
60	57.2	−72.5	34.0	0.33				
70	53.6	−73.8	35.7	0.16				
80	51.1	−74.0	37.3	0.18				
90	49.1	−74.9	41.7	0.32	49.0	−73.6	41.7	0.32
100	47.6	−76.0	47.3	0.28	47.4	−73.1	47.3	0.28
110	51.4	−74.1	50.8	0.30	50.9	−76.2	50.8	0.31
120	54.7	−72.1	54.5	0.25	53.8	−79.3	54.5	0.31
130	57.5	−70.1	58.3	0.24	56.3	−82.4	58.2	0.28
140	60.0	−68.1	62.3	0.25	58.4	−85. 6	62.2	0.30
150	62.2	−66.0	66.4	0.23	60.3	−88.7	66.3	0.24

Note. The Pacific finite rotation poles between 90 and 150 Ma (originally listed in supplementary Table DR1 in Steinberger & Gaina, 2007) are incorrect (see text), and they are here corrected with revised estimates of NR (in °/Myr) averaged over 10 Myr (e.g., 150–140 Ma in the row for 150-Ma age). Lat., Euler latitude (°); Long., Euler longitude (°).

(section 3). The motion of the Pacific plate was extended separately before 83.5 Ma using a smoothed version (i.e., some stage poles removed) of the WK08-A model of Wessel and Kroenke (2008). This smoothing resulted in comparatively low angular velocities for the Pacific plate (Figure 7c, red stippled line), but the pre-83.5 Ma Pacific finite rotations calculated in Matthews et al. (2016; GPlates default model 2.0/2.1) are problematic because of erroneous stage rotation calculations. Stage rotations in the time interval between t_1 and t_2 were computed by multiplying the inverse matrix for the finite rotation at t_1 and the matrix for the rotation at t_2, but this multiplication is noncommutative and was performed in the incorrect order (Table 1). This error is present in all public releases of GPlates, and because of this, the Pacific plate is rotated 39° clockwise (Figure 7b) in the time interval 140–150 Ma compared with the appropriate orientation of the Pacific plate [i.e., the Matthews et al., 2016 model extended correctly with the WK-08-A model; Table 3]. The Pacific is constructed from multiple triple junctions surrounding a steadily growing Pacific plate (Figure 2), which is initiated at 190 Ma according to the *Earthbyte* model (but remained stationary before 140 Ma). This error has considerable implications for the restoration and evolution of Panthalassic plate boundaries since almost all other plates in the Panthalassic Ocean are directly related by relative plate circuits to the Pacific plate before 83.5 Ma. Figure 8b highlights the large differences between the flawed and the correct reconstructions: The corrected *Earthbyte* model (Table 3) incorporates systematic clockwise rotations of the Pacific plate between 150 and 90 Ma (Figure 8b, *inset* figure), while in the flawed model these plate rotations are virtually absent. All other plates linked to the Pacific plate (e.g., Izanagi, Phoenix, and Farallon at 150–140 Ma), and the plate boundaries and triple-junctions in the corrected model are now in a counterclockwise position relative to their previous (flawed) orientations. Plate convergence directions along the margin of the Panthalassic Basin also vary substantially between the corrected and flawed model (Figure 8b).

The Wessel and Kroenke (2008) hot spot model assumes that the southern Shatsky Rise was emplaced above a stationary mantle plume at around 144 Ma (Figure 6c; thick yellow line), but the calculated hot spot track from the flawed *Earthbyte* model (Figure 6c; stippled yellow line) is very different from that expected from the original Wessel and Kroenke (2008) track: it does not link up the Shatsky and Hess rises and the track is also much longer. Published models incorporating the erroneous calculations of stage and finite rotations should not be used and the Pacific history must be reevaluated using the corrected rotations or new models that we provide here. This also calls for reevaluation of numerical models that were built upon the flawed reconstructions (i.e., all studies using GPlates for geodynamic exercises before 83.5 Ma).

Table 3
Absolute Motions for the Pacific Plate in a Mantle Reference Frame Since 95 Ma (Matthews et al., 2016) Based on a Smoothed Version of the WK08-A Model (Wessel & Kroenke, 2008), but the Rotation Poles Are Incorrect (See Text) and Are Here Corrected in the Right-Hand Column

Age	Pacific (Matthews et al., 2016)			Pacific corrected		
(Ma)	Lat.	Long.	Angle	Lat.	Long.	Angle
95	53.4	−77.5	52.7	52.9	−77.2	52.6
106.2	56.6	−73.5	59.1	57.2	−80.7	58.8
140	68.0	−58.3	74.0	58.2	−127.5	81.8
150	68.0	−58.3	74.0	58.2	−127.5	81.8

Note. In this model, the Pacific plate has no velocity between 190 and 140 Ma, and hence the 140 and 150 Ma rotation poles are identical. Lat., Euler latitude (°); Long., Euler longitude (°).

5. Toward Revised Pacific-Panthalassic Reconstructions Before 83.5 Ma

The Cretaceous is known for the high number of LIPs that erupted around the globe. The Shatsky Rise preserves evidence of volcanic activity 144-Myr old (Figure 9a), which coincides with chron M20 (our *preferred* time scale of Gee & Kent, 2007), or chron M18 in the time scale of Ogg (2012). The base of the M-series lineations (M0r) is tied to the Barremian-Aptian boundary and has age estimates in different time scales from ~114 Ma (Fiet et al., 2006) to ~126 Ma (Ogg, 2012). Geomagnetic polarity time scales favor a boundary age of ~121 Ma (e.g., Malinverno et al., 2012), coinciding with ^{40}Ar-^{39}Ar ages from M0r lavas in China (He et al., 2008), and supported by U-Pb ages from Barremian ash layers in Svalbard, which demonstrate that the Barremian-Aptian boundary must be younger than 123 Ma (Midtkandal et al., 2016).

Table 4
Absolute Motions for the Pacific Plate (Finite Euler Rotation Poles) in a Mantle Reference Frame and Stage Poles Since 83.5 Ma (Models S and R), for Example the Stage Pole for the 95–83.5 Ma Interval Is Listed in the 95 Ma Row

	Finite Euler rotation poles			Stage poles		
Age (Ma)	Latitude (°)	Longitude (°)	Angle (°)	Latitude (°)	Longitude (°)	Angle (°)
Model S						
83.5[a]	−55.38	104.40	−47.29			
95	−53.66	102.34	−53.82	39.37	−79.92	6.77
100	54.38	−78.39	56.53	59.64	−105.65	2.82
123	60.21	−78.53	63.72	71.10	−175.04	9.26
144	62.73	−66.10	69.29	58.82	50.22	8.99
150[b]	*63.23*	*−62.21*	*71.17*	*58.82*	*50.22*	*2.83*
Model R						
83.5[a]	−55.38	104.40	−47.29			
90	−54.00	103.88	−52.10	41.00	−71.93	4.95
95	−53.68	102.47	−54.00	35.37	−95.33	2.07
100	55.52	−79.00	55.52	52.16	170.32	2.40
110	57.86	−78.79	58.64	75.35	−167.49	3.84
123	59.01	−78.59	64.37	68.42	−92.36	5.85
130	58.75	−74.49	67.01	52.32	−0.04	3.51
135	58.62	−71.86	68.80	54.29	4.09	2.36
144	62.73	−66.10	69.29	34.21	111.05	5.66
150[b]	*65.27*	*298.61*	*69.84*	*34.21*	*111.05*	*3.77*

Note. Finite Euler rotation pole at 83.5 Ma from GMHRF-3 (Doubrovine et al., 2012). Model R is implemented in Appendix 1 data-file *Pacific.ZIP*.
[a]GMHRF-3 (Doubrovine et al., 2012). [b]Extrapolated.

The seafloor surrounding the Shatsky Rise reaches depths of more than 5,000 m (Amante & Eakins, 2009), and three major volcanic massifs with a north-east trending age progression—Tamu (~144 Ma), Ori (~142-140 Ma), and Shirshov (~137–136 Ma; Figure 9a)—rise to water depths of 3,200–2,000 m (e.g., Sager et al., 1988; Nakanishi et al., 1989, 1999; Sager, 2005; Tejada et al., 2016). The initial emplacement of the Shatsky Rise (Tamu Massif) may have caused major plate boundary reorganizations (e.g., Nakanishi et al., 1989, 1999), including a major eastward jump (~800 km) of the Pacific-Izanagi-Farallon triple junction, and a noteworthy change (~25°) of the Pacific-Izanagi seafloor spreading direction (Figure 10). Recently, it has been argued that this important reorganization began earlier, around M23–M22 time (~151–147 Ma; time scale of Gee & Kent, 2007) and that the Tamu Massif (~144 Ma) formed near the Pacific-Farallon-Izanagi triple junction (Sager et al., 2016). In other words, did the initial Shatsky plume cause the triple junction to jump, or did it erupt into an actively spreading triple junction? The latter scenario (unless a coincidence) can be explained by "upside-down drainage" (Sleep, 1997), whereby melts were transported toward the spreading center (Figure 10f), which was later followed by a jump of the spreading ridge toward the plume (Figure 10g; explored in detail in section 7).

Table 5
Absolute Motions for the Pacific Plate in a Mantle Reference Frame by Extending the Earthbyte Model (Matthews et al., 2016) With Our New Pacific Model R Stage-Poles From 83 Ma (Implemented in Appendix 1 Data-File Pacific_EARTHBYTE_Model_R.ZIP)

Age (Ma)	Finite Euler rotation poles		
	Latitude (°)	Longitude (°)	Angle (°)
83.0	53.79	−75.33	47.46
90	52.55	−75.77	52.29
95	52.29	−77.10	54.21
100	54.17	−78.48	55.69
110	56.58	−78.20	58.76
123	57.85	−77.92	64.46
130	57.61	−73.93	67.09
135	57.50	−71.37	68.88
144	61.60	−65.75	69.25
150[a]	*64.14*	*−61.19*	*69.73*

[a]Extrapolated.

In mantle plume models, suggested hot spot tracks (volcanic paths) linking the Shatsky and Hess Rises include fitting a path running northward from the Shatsky Rise along the Papanin Ridge and then returning south-eastward toward the Hess Rise (Sager, 2005; Figure 9a; Shatsky North in Figure 6a), or a hot spot track (Shatsky South in Figure 6a) that links the Shatsky and Hess Rises more directly via the Ojin Rise seamounts after 137 Ma (red stippled arrow in Figure 9a; see Tejada et al., 2016). Altered trachyte samples from the Hess Rise DSDP Site 465A (Figure 9a) yield $^{40}Ar/^{39}Ar$ ages of 90–94 Ma (Pringle & Dalrymple, 1993), but these must be

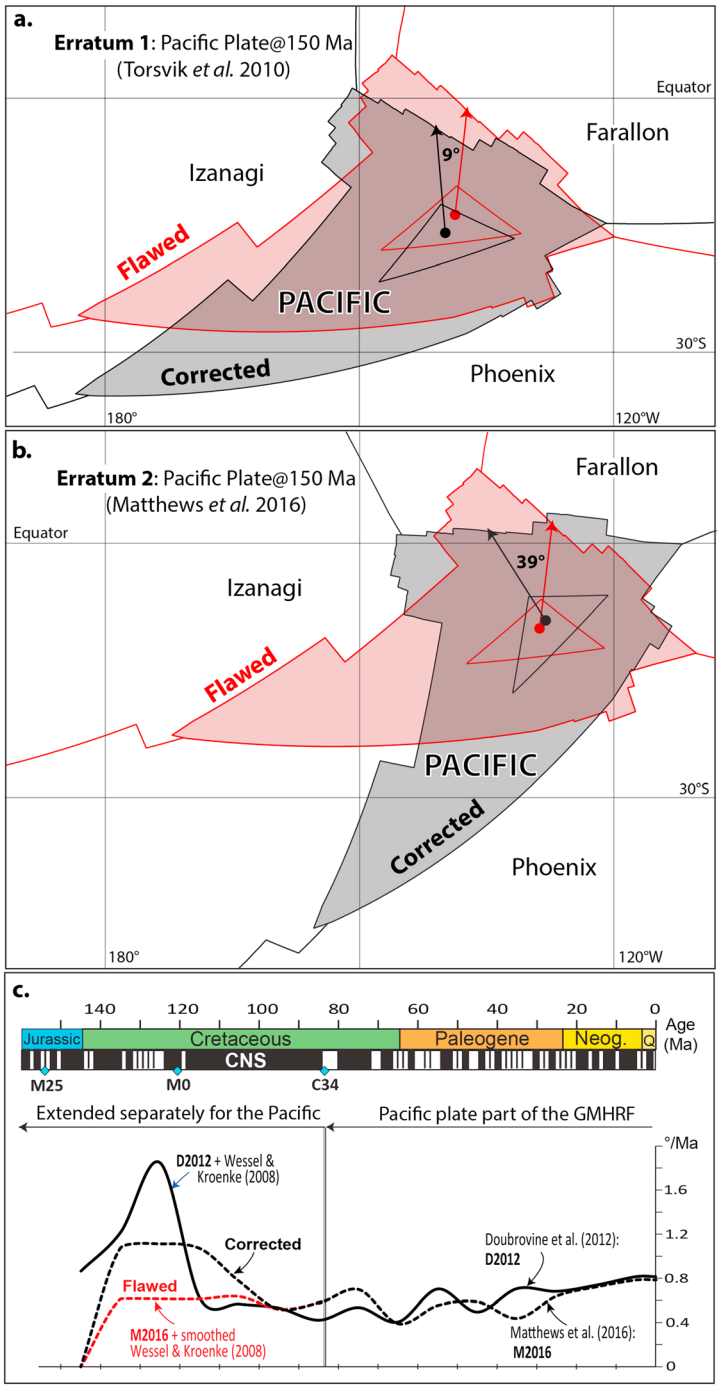

Figure 7. (a) The original reconstruction of Torsvik et al. (2010) for the Pacific plate at 150 Ma (red polygon and lines) and the corrected reconstruction (black polygon and lines). The smaller black and red triangles are the approximate size of the Pacific plate at 180 Ma and the black and red arrows show the present north direction. The corrected reconstruction (see text) is rotated 9° compared with the erroneous version. The Pacific and networked plates (Izanagi, Farallon, and Phoenix) were reconstructed back to 150 Ma with stage poles listed in Duncan and Clague (1985). (b) The original reconstruction of Matthews et al. (2016) for the Pacific plate at 150 Ma (red polygon and lines) and the corrected reconstruction (black polygon and lines). The corrected reconstruction (see text) is here rotated 39° compared with the erroneous version. The Pacific and networked plates based on finite rotation poles listed in Wessel and Kroenke (2008). (c) Jurassic to Recent time scale, magnetic polarity (Gee & Kent, 2007; isochrons M25, M0, and end of C34 highlighted) and angular velocity for the Pacific plate based on Doubrovine et al. (2012) and Matthews et al. (2016). Both models extended separately for the Pacific using the WK08-A model of Wessel and Kroenke (2008), which yields an angular velocity peak of nearly 2°/Ma between 120 and 130 Ma. The Matthews et al. (2016) model yields substantially lower angular velocities, but the model is flawed (red stippled) and the corrected model almost doubles Mid-Cretaceous angular velocities. Note also that the Matthews et al. (2016) model is a heavily smoothed version of WK08-A (arbitrarily removed several rotation poles), and thus, the angular velocities are much lower than those calculated from Doubrovine et al. (2012).

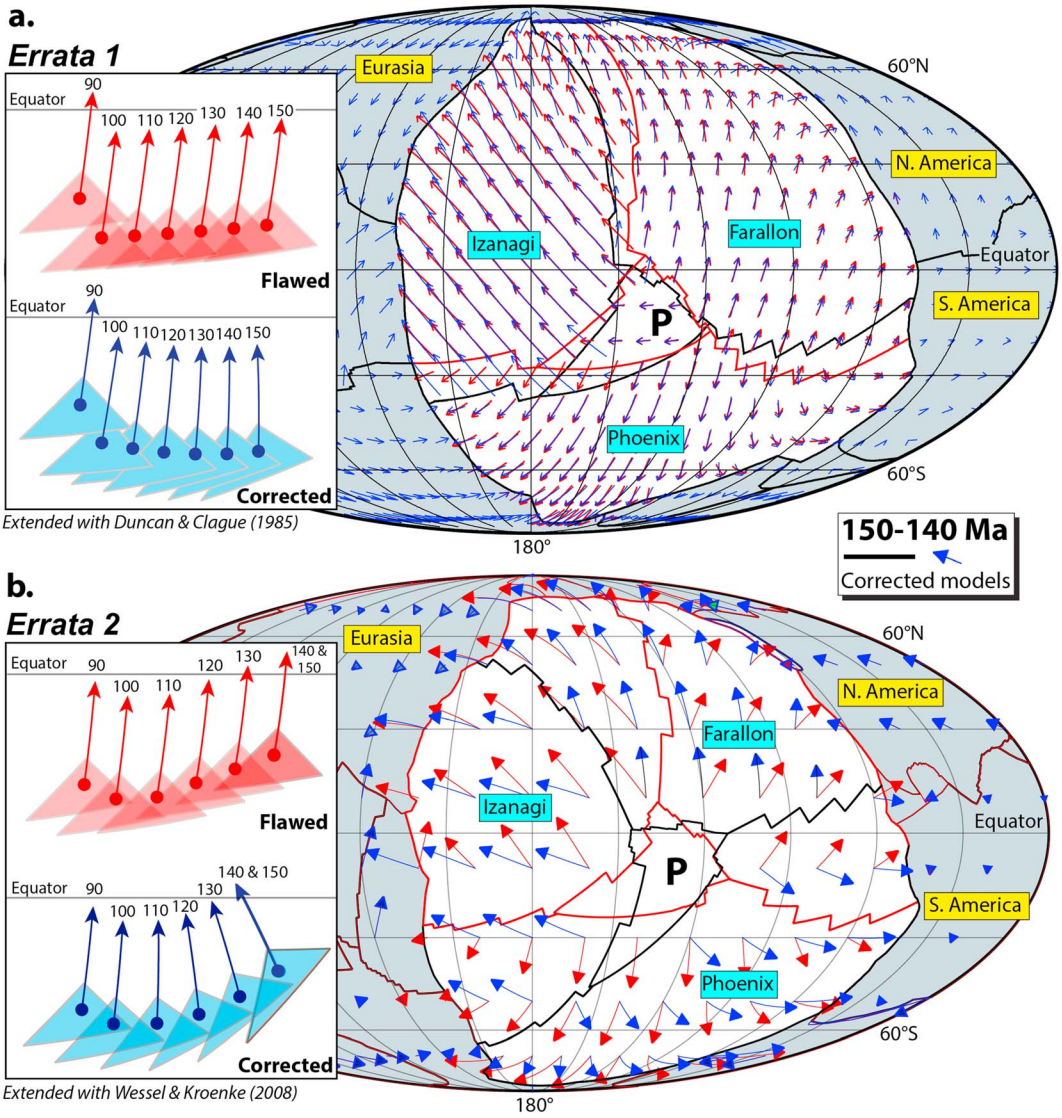

Figure 8. (a) The reconstruction of Torsvik et al. (2010) at 150 Ma with correction for the Pacific plates based on Duncan and Clague (1985). The erroneous Pacific reconstruction shown with red plate boundary lines and red vector arrows (see Erratum 1 in text). (b) The reconstruction of Matthews et al. (2016) at 150 Ma with correction for the Pacific plates based on Wessel & Kroenke (2008, WK08-A model). The erroneous Pacific reconstruction shown with red plate boundary lines and red vector arrows (see Erratum 2 in text). In this reconstruction, Izanagi is the largest plate at 150 Ma (~16% of Earth surface) and along with Farallon, Phoenix, and Pacific plates covers ~46% of the Earth's surface. Note that plate polygons differ between the two models. It is interesting to note that the original reconstructions in panels a and b (the flawed ones with red lines) are very similar, while the corrected models differ substantially and impose a clockwise Early-Mid Cretaceous rotation. *Inset* diagrams show the reconstruction of the Pacific plate (approximately the shape of the Pacific plate at 180 Ma in the model of Matthews et al., 2016) and the blue (corrected models) and red (erroneous models) arrows show the orientation of the present north direction. P, Pacific plate.

considered minimum ages as the dated Hess Rise trachytes are overlain by (older) Late Albian sediments; the Hess Rise is therefore ~100 Ma or older. Hess Rise may represent a second phase (as predicted in Bercovici & Mahoney, 1994) of massive upper mantle melting and magmatic outpouring above the plume that once formed the Shatsky Rise, perhaps similar to the ~135 Ma Parana-Etendeka LIP and Rio Grande Rise (80–90 Ma) in the South Atlantic (Bercovici & Mahoney, 1994; Torsvik et al., 2009), or the North Atlantic Igneous Province (peaking at ~55 Ma) and the Paleogene-Neogene magmatic phase of Iceland (Torsvik et al., 2015).

The Mid-Pacific Mountains (Figure 9b) is an oceanic plateau with an enriched OIB geochemical signature (Chen & Liu, 2018), which is situated about 1,500 km south of the Hess Rise. Ernst (2014) assumed an emplacement age of 130 Ma (oldest known date is 128 Ma, $^{40}Ar/^{39}Ar$; Pringle & Duncan, 1995), while Madrigal

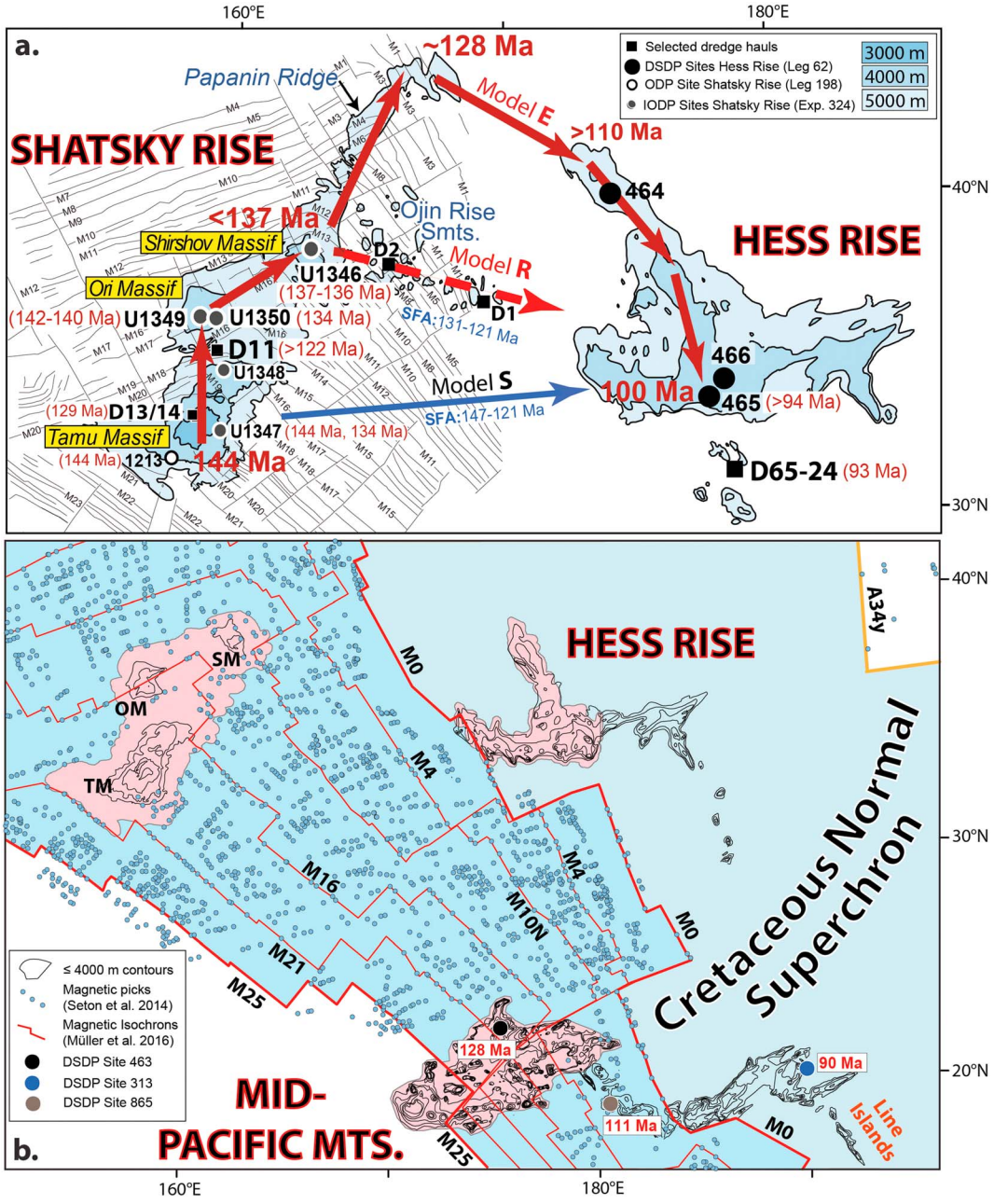

Figure 9. (a) Shatsky and Hess Rise oceanic plateaus (after Tejada et al., 2016) with $^{40}Ar/^{39}Ar$ ages from drill and basement dredging sites (Geldmacher et al., 2014; Heaton & Koppers, 2014; Koppers, 2010; Mahoney et al., 2005; Pringle & Dalrymple, 1993). The Tamu Massif, the oldest volcano of the Shatsky Rise (~144 Ma), and perhaps the single largest volcano on Earth (Sager et al., 2013), has been suggested as a likely plume location during the initial eruption of Shatsky. We show two suggested paths of volcanism (red thick lines with arrowheads) between Shatsky and Hess, that is, Model R (Sager et al., 1999; Tejada et al., 2016) and Model E (Sager, 2005). The age range for the red stippled line (Ojin Rise seamounts) and the estimated age at the northern end of the Papanin ridge are estimated seafloor ages (SFA). A simple direct connection between SW Shatsky and Hess Rise (essentially the model of Duncan & Clague, 1985) is shown by the blue arrow. Magnetic lineations in the vicinity of Shatsky Rise after Nakanishi et al. (1999). (b) Magnetic picks (Seton et al., 2014) and default magnetic isochrons in GPlates 2.0 and 2.1 (Müller et al., 2016). The area is here extended southward to include the Mid-Pacific Mountains with some $^{40}Ar/^{39}Ar$ ages from drill sites (Pringle & Duncan, 1995; see also Winterer & Sager, 1995). We show 4,000-m water depth contours or less (500-m intervals), the typical large igneous province (LIP) outlines for Shatsky and Hess Rises, and we have indicated the extent of the Mid-Pacific Mountains (Mts) LIP (light pink shading). We have removed depth contours associated with the Hawaiian-Emperor Chain in both panels. OM, Ori Massif; SM, Shirshov Massif; TM, Tamu Massif (see panel a). M-series isochrons include M25 (153.43–154.00 Ma), M21 (145.52–146.56 Ma), M16 (136.49–137.85 Ma), M10N (129.63–130.49 Ma), M4 (125.67–126.57 Ma), and MO (120.6 Ma) using time scale of Gee and Kent (2007).

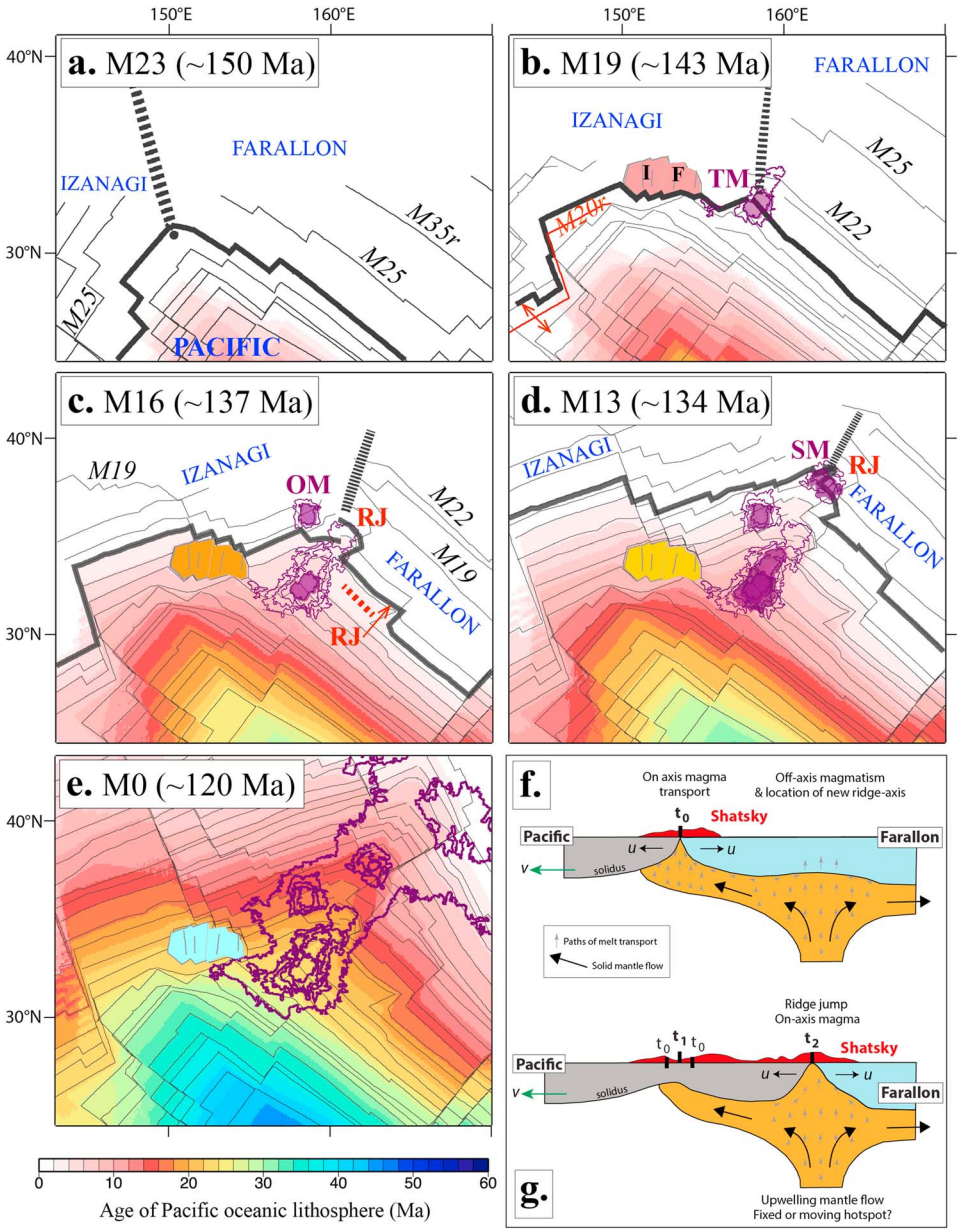

Figure 10. (a-e) Late Jurassic-Early Cretaceous evolution of oceanic lithosphere (in a fixed Pacific plate reference frame) in the Shatsky Rise area (NW Pacific) based on isochrons (thin black lines) constructed from magnetic anomalies (Huang et al., 2018; Nakanishi et al., 1999), and tectonic features identified from gravity anomaly grid (Sandwell et al., 2014). Conjugate isochrons on Izanagi and Farallon plates were modeled using the rotations of Seton et al. (2012) and Wright et al. (2016); the location of the paleo-plate boundary between Izanagi and Farallon (thick dashed line) is inferred from plate tectonic rules: Relative motions are known at the two plate boundaries where isochrons have been preserved. Then they can be determined at the third boundary by vector addition, and the direction of the spreading boundary can be inferred if it is orthogonal to the direction of relative motion. Ridge jumps (RJ) and relocation of the triple junction between the Pacific, Izanagi, and Farallon plates are shown. A piece of Izanagi (I) and Farallon (F) oceanic lithosphere transferred to the Izanagi plate after the eastward jump of the triple junction before M19 time is shown as a polygon with different age (and therefore different color) in panels b-e. Both pieces transferred to the Pacific plate at around M16 time (panel c). The Shatsky Rise and identified volcanic centers (OM, Ori Massif; SM, Shirshov Massif; TM, Tamu Massif) are outlined by the bathymetric contours (dark magenta) extracted from ETOPO1 global bathymetry (Amante & Eakins, 2009). M-sequence lineations in the NW Pacific are termed the Japanese lineations, and there is a clear strike change at around M20 time. Time-slices and annotated anomalies include M35 (162.49–162.55 Ma), M25 (153.43–154.00 Ma), M23 (150.04–150.93 Ma), M22 (147.06–148.79 Ma), M20 (143.36–144.7 Ma), M19 (141.63–143.07 Ma), M16 (136.49–137.85 Ma), and M13 (134.08–134.27 Ma) using time scales of Gee and Kent (2007) and Ogg (2012). (f, g) Simple model for a near-ridge mantle plume, melting, melt transport, and magmatic heating of the lithosphere (adapted from Mittelstaedt et al., 2011). In this model, the Shatsky plume initially impinged the Farallon (partly Izanagi?) lithosphere but melt was transported south-westward and the Tamu Massif (144 Ma) was emplaced atop the Pacific-Izanagi-Farallon triple junction at time $\mathbf{t_0}$. Eventually, melts from the Shatsky plume may have directly penetrated the oceanic lithosphere leading to ridge jumps and relocation of the triple junction at time $\mathbf{t_2}$. A Pacific plate moving southwestward (as in our model) and a quasi-stationary hot spot may have resulted in additional ridge jumps and relocation of the triple-junction until about M13 time. In the process, essentially all of the Shatsky Rise plume-related volcanism was transferred to the Pacific plate (see text).

et al. (2016) used an initial LIP age of 140 Ma ("magnetic anomaly age") for the main westerly volcanic constructs. Eastward the Mid-Pacific Mountains show a curvature that becomes younger to about 90 Ma (Figure 9b), and connects southward with the Line Islands Chain; together those features have been interpreted as a hot spot track for decades (e.g., Engebretson et al., 1985; Morgan, 1972a).

Doubrovine et al. (2012) tested the Pacific plate absolute motion from 83.5 to 120 Ma by using both the Duncan and Clague (1985) and Wessel and Kroenke (2008; WK08-A) models; both models were implemented correctly in Doubrovine et al. (2012). We have here extended the Doubrovine et al. (2012) model to 150 Ma (using the Torsvik et al., 2010, plate polygon model) with the WK08-A model, which not only implies high Pacific plate angular velocities (Figure 7c), but systematic clockwise rotations between 150 and 100 Ma (Figure 8b *inset* diagram) and high NR (see section 5.1) as the Izanagi-Farallon-Phoenix plates are kinematically linked with the Pacific plate. We therefore devise here a new absolute Pacific plate model from 83.5 to 150 Ma using a fixed hot spot approach coupled with paleomagnetic (latitude) data from three Pacific LIPs while simultaneously minimizing absolute plate velocities and NR. Such a combined approach is not trivial (or unique). Minimizing NR was simply achieved by *not* rotating the Pacific plate around a "local" rotation pole (i.e., one located within or near the plate polygon itself as seen in the WK08-A model), and palaeomagnetic data must be corrected for TPW to check and refine an initial hot spot approach based on the geometry and ages from seamount chains (and LIP outlines). Our starting model was the Doubrovine et al. (2012) model extended to 150 Ma with the WK08-A model and we used TPW corrections predicted from the Indo-Atlantic domain (Torsvik et al., 2012; see example in Figure 4) to estimate LIP paleolatitudes in a mantle frame (insensitive to TPW).

Paleolatitudes from the Pacific plate can be derived from sediment and basalt cores, but we only examine paleomagnetic data collected from volcanic rocks (Shatsky Rise, Ontong Java Plateau, and Hess Rise) and not from sediments, because the latter may be prone to inclination shallowing effects (e.g., Bilardello & Kodama, 2010a, 2010b; Domeier et al., 2012; Kent & Tauxe, 2005; Kodama, 2009; Tauxe, 2005; Torsvik et al., 2012). The Shatsky Rise erupted at around 144 Ma (Mahoney et al., 2005; Tejada et al., 2016), and there are younger volcanics (141–134 Ma; Figure 9a) with paleomagnetic data that collectively yield local paleolatitudes between 3°N and 10°N (±20°; Figure 11) in the paleomagnetic reference frame (Sager et al., 2015; Tominaga et al., 2005). Owing to these low paleolatitudes and ambiguities in the polarity of the paleomagnetic data, Tominaga et al. (2012) argued that the Shatsky Rise initially erupted at low southerly latitudes at 144 Ma and then drifted across the equator, but we model all the volcanic rocks of the Shatsky Rise to have erupted in northerly latitudes (see also Sager et al., 2015). Paleomagnetic sites from the Ontong Java Plateau are dated to ~123 Ma and the local paleolatitudes of 18 $^{+4.5}/_{-4.1}$°S to 28 $^{+14.1}/_{-10.3}$°S (Riisager et al., 2003) are used to constrain the latitude of the Pacific plate at that time. Finally, Hess Rise erupted at low northerly latitudes at ~100 Ma (Figure 11).

Following previous studies (e.g., Bercovici & Mahoney, 1994; Duncan & Clague, 1985; Sager, 2005; Sager et al., 1999; Wessel & Kroenke, 2008), we consider that the Shatsky and Hess rises may have been sourced from the same hot spot (now extinct) and assume that the source plume originally impinged the oceanic lithosphere beneath the Shatsky Rise (Figure 9a) at 144 Ma, and later beneath the Hess Rise at ~100 Ma. Using these and other constraints, we have tested three new Pacific models with varying degrees of complexity.

5.1. Model S (Simple)

Model S is our simplest model where we connect the Shatsky and Hess rises in a direct manner between 144 and 100 Ma (Figure 12a), which bears similarities to the Duncan and Clague (1985) model (Figure 6c). Modeled paleomagnetic latitudes (including the Ontong Java Plateau at 123 Ma) are within errors of the observed latitudes (Figure 11), and we ensured that the Pacific plate is *not* rotating around a "local" rotation pole, that is, that the rotation pole is far—close to 90°—away from the reconstructed plate location, in order to keep NR small, because such "local" rotations are poorly constrained by hot spot tracks on the plate. The resulting Pacific plate motion path resembles that of Duncan and Clague (1985), but Model S yields lower average Pacific plate angular velocities (<0.45°/Ma; Figure 13a). Compared with the Duncan and Clague (1985) and WK08-A model, NR is significantly reduced before 100 Ma (NR mean = 0.17 ± 0.06°/Ma), and is comparable with values for the past 50 Myrs (Figure 13b).

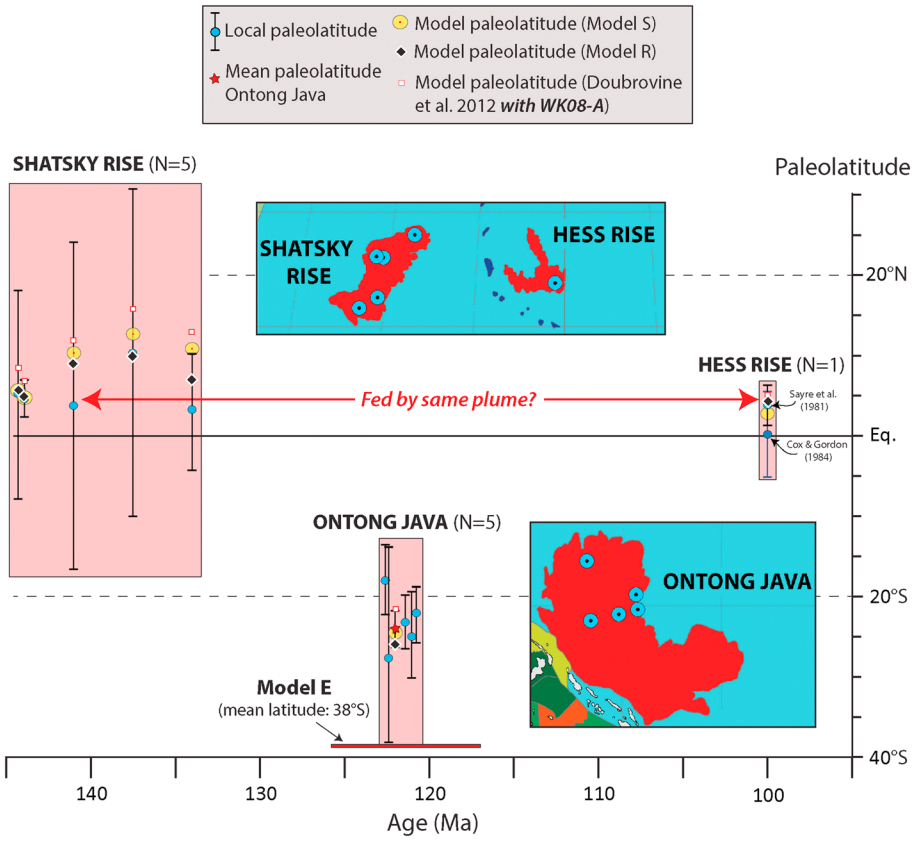

Figure 11. Local paleolatitudes (blue circles) with error bars (95% confidence) derived from paleomagnetic data from volcanics rocks from Shatsky Rise, Hess Rise, and Ontong Java Plateau. These are compared with latitudes derived from our Pacific Model S (large yellow circles), Model R (black/white diamonds), and the original model of Doubrovine et al. (2012; white boxes) using the WK08-A (Wessel & Kroenke, 2008) Pacific extension. Paleolatitudes in all models are recalculated to the local sampling site for direct comparison. Models E and R are similar for Shatsky and Hess Rises but Model E latitudes for Ontong Java Plateau are statistically different from the observed latitudes. Inset maps: Paleomagnetic sampling locations of volcanic rocks from Shatsky Rise (EXP 324: Site U1350, U1346, U1349, U1347; Sager et al., 2015 & Hole 1213B; Tominga et al., 2005), Ontong Java Plateau (LEG 192: Site 807, Hole 1183, Hole 1185, Hole 1186, Hole 1186; Riisager et al., 2003) and Hess Rise (Hole 465, Leg 62; Sayre, 1981; recalculated in Cox & Gordon, 1984).

The 95–85 Ma plate motion path in Model S parallels the Wentworth-Musicians seamount chains (as in the Duncan & Clague, 1985, and WK08-A models), where the Musicians seamount chain has traditionally been considered a hot spot track with a rather clear time progression between 96 and 76 Ma (Figure 6b). Surprisingly, this time progression was recently questioned by much younger $^{40}Ar/^{39}Ar$ ages along the southern Musicians ridges (O'Connor et al., 2015). The Musicians seamount chain was therefore not used as a direct input in Model S, but the Pacific plate motion is near parallel to the Musicians (and Wentworth) seamount chain between 95 and 85 Ma (Figure 12a).

5.2. Model R (Refined)

In a more refined model (Model R) we attempt to build a Pacific plate motion path that assumes that the northeast trend for the Shatsky Rise is a real hot spot track that then parallels the Ojin Rise Seamounts toward the Hess Rise (red dashed line in Figure 9a; Sager et al., 1999; Tejada et al., 2016). We also attempted to reproduce the curvature of the Mid-Pacific Mountains from ~128 to 90 Ma (Figure 9b) and to parallel the Musicians, Wentworth, and Line Islands chains from 95 to 83.5 Ma (i.e., before crossover to GMHFR-3). Modeled paleomagnetic latitudes fit well with the observations (Figure 11), and both NR (mean = 0.18 ± 0.04°/Ma between 150 and 90 Ma) and Pacific plate velocities (mean = 0.46 ± 0.09°/Ma, corresponding to ~5 cm/year) are low and reasonable (Figure 13).

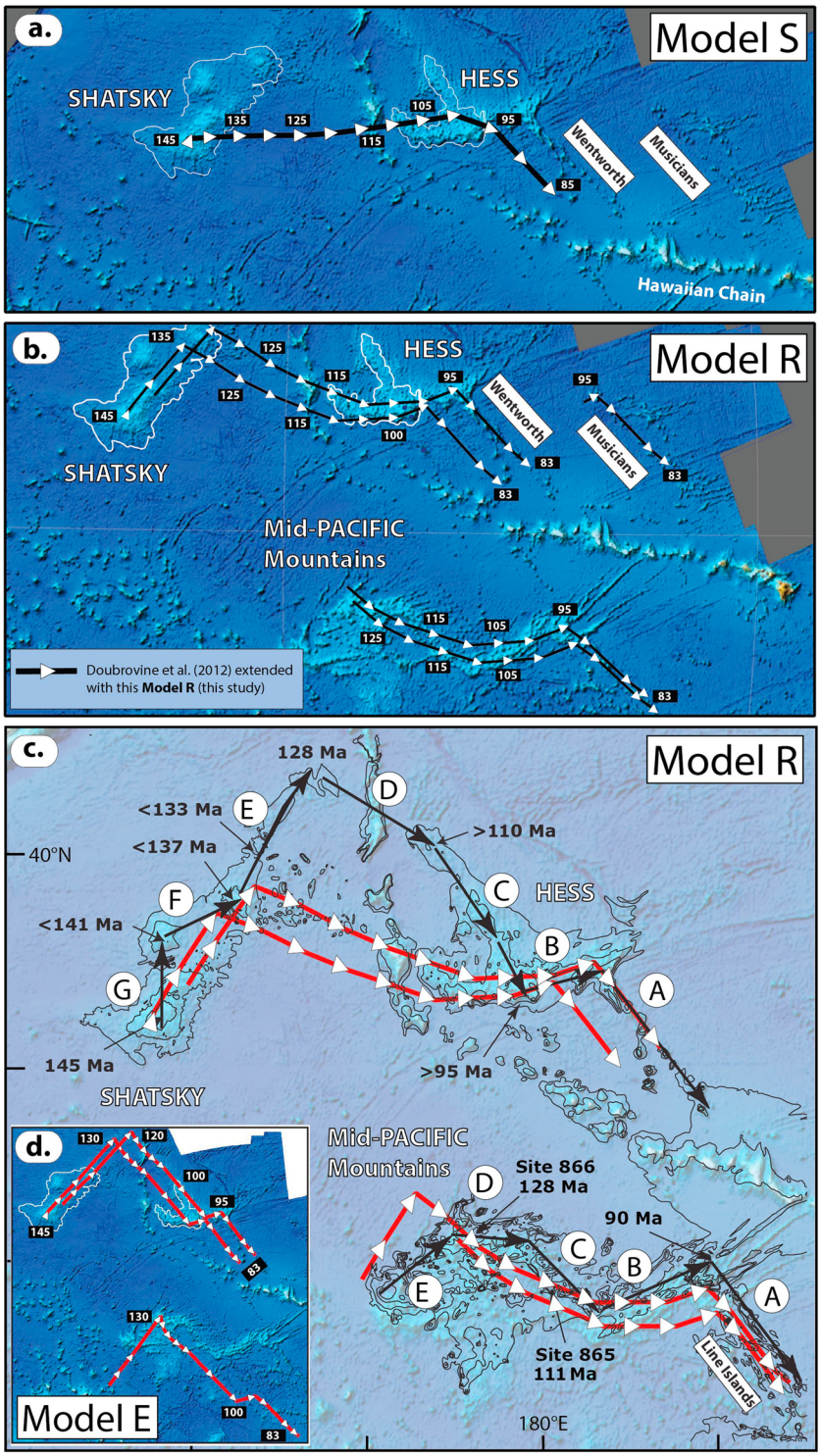

Figure 12. (a) Predicted Pacific plate motion track with Model S for a direct connection between Shatsky and Hess Rises. (b, c) Predicted Pacific plate motion tracks (Model R) for Shatsky and Hess connection, Wentworth and the Musicians chains and the Mid-Pacific Mountains. The volcanic and age trends in the Shatsky Rise-Hess Rise pair and the Mid-Pacific Mountains have certain similarities and arrows show trends, with labeled segments (panel c) to show correlation between the two lineaments, both showing a *lopsided "M" shape* with similar ages at analogous points (Sager, 2005). Ages from Mid-Pacific Mountains detailed in Winterer and Sager (1995) and the 1,000-m bathymetry contours shown for reference. Model R reproduces the trajectory of the Mid-Pacific Mountains quite well. (d) Predicted plate motion track with Model E. Model E fails to reproduce the trajectory of the Mid-Pacific Mountains (segments A to E). All models extended from GMHRF-3 (Doubrovine et al., 2012) before 83.5 Ma.

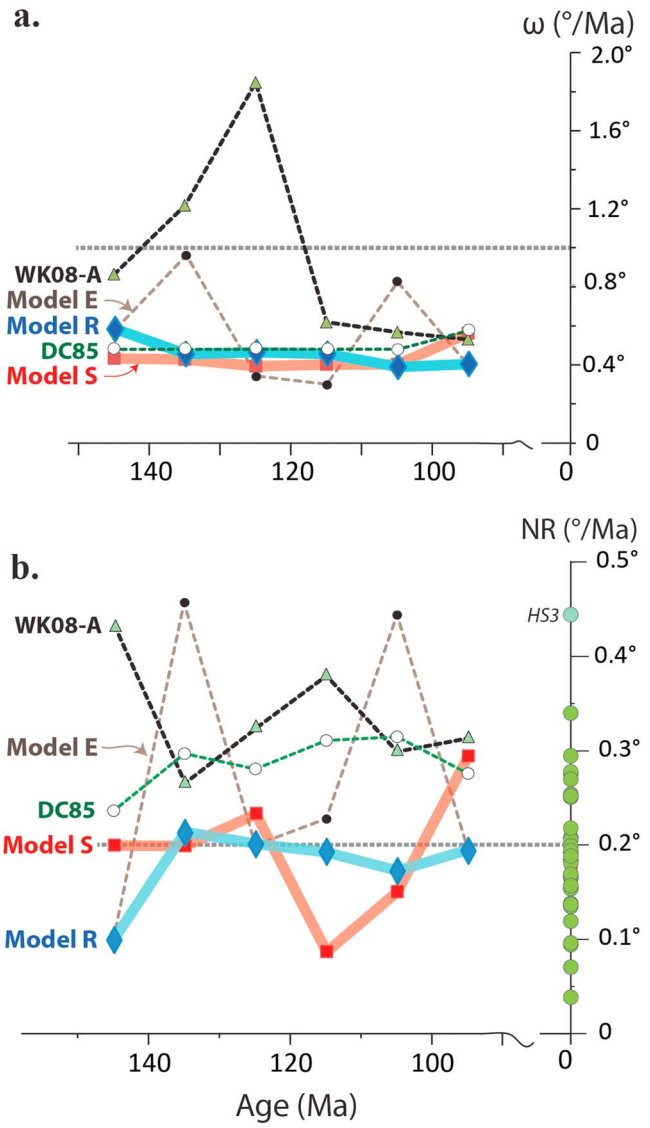

Figure 13. (a) Absolute angular velocities for five different Pacific plate models from 150 to 90 Ma. The models are WK08-A (Wessel & Kroenke, 2008), DC85 (Duncan & Clague, 1985), and Models S (simple), R (refined), and E (extreme) developed in this study. All velocities calculated over 10-Myr intervals (e.g., 150–140 Ma, 100–90 Ma). (b) Net lithosphere Rotation (NR) calculated for the different mantle reference frames but two different plate polygon models. WK08-A and DC85 calculated from the plate polygon model of Torsvik et al. (2010) while Models S, R, and E use modified plate polygons from Matthews et al. (2016). NR values calculated over 10-Myr intervals (e.g., 150–140 and 100–90 Ma). NR values (green filled circles) plotted on zero-age axis are NR estimates for recent times (averaging to 0.21 ± 0.06 °/Ma) based on plate/geodynamic models (after Wang et al., 2018). After removing the two highest values, model SKS (from Becker et al., 2015, but not supported by those authors; not shown, off scale) and model HS3 (Gripp & Gordon, 2002) then NR averages to 0.19 ± 0.05°/Ma.

For Model R, we show several synthetic tracks (Figures 12b and 12c). The most southerly Shatsky Rise track can be viewed as a plume impinging directly below the Tamu Massif at ~144 Ma with parts of the Shatsky Rise interpreted as a NE-orientated hot spot track to about 135 Ma. Such a scenario, for example, is compatible with a plume-induced reorganization of the Pacific-Farallon-Izanagi triple junction. The northerly Shatsky track is compatible with a more complex scenario where the initial plume center at ~144 Ma was located ~250 km north of the Tamu Massif. This path traces the Shatsky Rise north-eastward until ~135 Ma, then traces the Ojin Rise Seamounts to Hess Rise, and finally reproduces the Wentworth Chain after 95 Ma. In this model, the Shatsky plume initially impinged the Farallon Plate but the first magmatic outpourings were diverted southwestward by upside-down drainage into an active triple junction (Figures 10b and 10f). Later, the plume directly penetrated the oceanic lithosphere, leading to a NE-directed ridge jump and relocation of the triple junction above the plume conduit (Figure 10g). Further plume-induced relocation of the triple junction may then have occurred when the Pacific plate was moving in a southwest direction over a quasi-stationary plume to about 135 Ma (see section 7).

We also show two synthetic tracks for the Mid-Pacific Mountains: one starts at DSDP Site 866 (dated to 128 Ma); it reproduces the curvature of the Mid-Pacific Mountains reasonably well and subsequently tracks southward toward the Line Islands after 95 Ma. A second and more northerly track also reproduces the Mid-Pacific Mountains but is extended back to 145 Ma (Figure 12c) to test Model E discussed in the next section.

5.3. Model E (Extreme)

In this model, we attempt to reproduce a suggested volcanic path (Sager, 2005) starting northward from Shatsky Rise along the Papanin Ridge and then returning southeastward toward the Hess Rise (Figure 9a). It is possible to build such a model that fits segments A–G connecting Shatsky and Hess rises (Figure 12c), but Model E fails to reproduce the trajectory of the Mid-Pacific Mountains (segments A to E; Figures 12c and 12d). Because of major adjustments in the reconstructed latitudes, Model E *fails* to reproduce the paleomagnetic latitudes provided by the Ontong Java Plateau at around 123 Ma (Figure 11), and we dismiss this model. Also, note that this model produces a spiked angular velocity and NR pattern (Figures 13a and 13b) with NR peaks around 0.45°/Ma and peak angular velocities at around 1°/Ma (approximately 10 cm/year).

6. Model R at Work

Models S and R yield low values for plate velocities and NR, they are both consistent with LIP paleolatitudes derived from paleomagnetic data, but we consider Model R as the best and most realistic model. The motion of the Pacific plate between 90 and 150 Ma is schematically illustrated in Figure 14, in both mantle and paleomagnetic frames for Model R. In the mantle frame, the Pacific plate drifted southwestward between 150 and 135 Ma (Figure 14a) at angular velocities of ~0.3–0.4°/Ma (Figure 13a). Compared with the *corrected* WK08-A model (Figure 8b *inset* diagram) we assured that our model did not include systematic *local* rotations of the Pacific plate and thus NR for Model R is reduced to 0.2°/Ma or lower (Figure 13b). Between 135 and 90 Ma the Pacific plate drifted slowly (~0.4°/Ma) in a northwesterly direction and NR was below 0.2°/Ma. The mantle (Figure 14a) and paleomagnetic (Figure 14b) frames differ because of TPW; one pronounced counterclockwise phase between 150 and

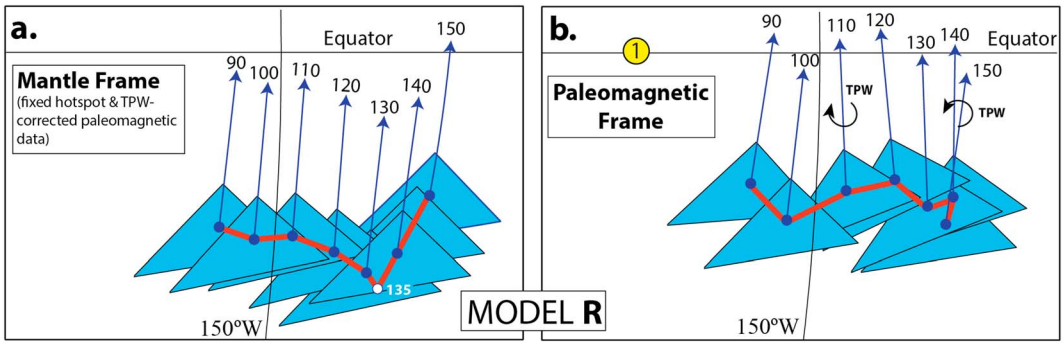

Figure 14. (a) Mantle frame reconstructions (Model R) of the Pacific plate (approximate size and shape of the Pacific plate at 180 Ma) and the blue arrows with numbers (Myrs) are the present day north direction. Shown in 10-Myr intervals but a central location of the Pacific plate is also shown at 135 Ma (white circle), because the Pacific plate changes in direction at this time. (b) As in panel a but here reconstructed in a paleomagnetic frame, and TPW rotations obey the global ("continental") estimates as in Figure 4. Open yellow circle (marked 1) is the center for TPW (0°N, 169°W).

140 Ma (Figure 4), and a second clockwise phase between 110 and 100 Ma, both of which occurred about an equatorial axis positioned at 169°W, or its antipode 11°E with opposite sense of rotation (Torsvik et al., 2012).

The southern parts of the Shatsky Rise (Tamu Massif) were emplaced near the Pacific-Izanagi-Farallon triple junction at ~144 Ma (Figures 15a and 10b). The Shatsky plume may have impinged the base of the *Farallon*

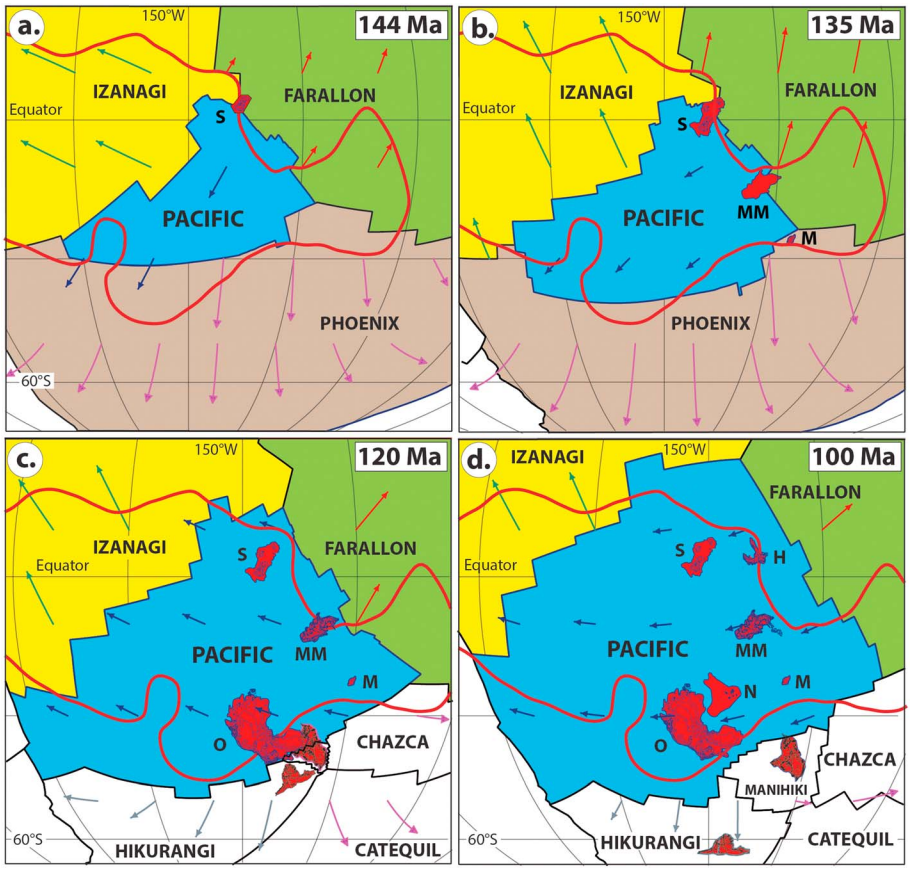

Figure 15. Mantle frame reconstruction and plate velocity vectors of the Pacific (Model R) and networked plates from 144 to 100 Ma (zoomed in Mollweide projections). The thick red line is the JASON plume generation zones (correspond to the 0.9% slow contour in the *s10mean* tomography model; Doubrovine et al., 2016). Red-shaded polygons are typically used large igneous province outlines for Shatsky Rise (S), Magellan Rise (M), Ontong Java (O), Manihiki and Hikurangi Plateaus, the Nauru Basin (N), and the Hess Rise (H). Here we use the 4,000-m depth contour to define the Mid-Pacific Mountains (MM) LIP. Light blue lines inside the large igneous province shaded polygons are depth contours ≤4,000 m.

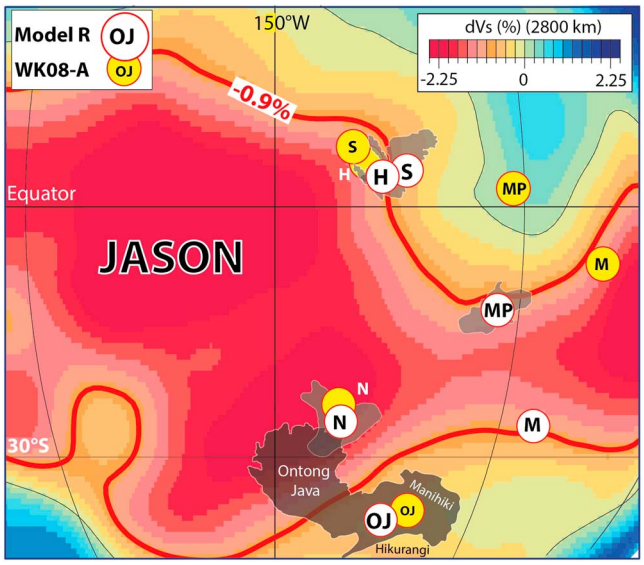

Figure 16. The "six" Pacific large igneous provinces (LIPs; see text) reconstructed with our new Pacific Model R (white-shaded annotated circles) and the WK08-A model (smaller yellow-shaded circles). Reconstructed LIPs are draped on the *s10mean* tomography model (2,800-km depth) where the plume generation zones (PGZ, thick red line) approximates the 0.9% slow contour (Doubrovine et al., 2016). Reconstructed LIP centers plot on average at 3.2 ± 2.8° (Model R) or 6.2 ± 4.2° (WK08-A) from the PGZ. Linking surface and deep mantle heterogeneities obviously depends on several factors, including LIP age uncertainties and the choice of both plate and tomography models. In addition, plumes may have been advected by the convecting mantle as they ascended through it, and a LIP eruption site may not mark precisely where a plume impinged on the base of the lithosphere (e.g., Figure 10f). Locating plume eruption centers with higher resolution than ~500 km may sometimes be unrealistic (Torsvik et al., 2006). Annotated LIP centers: H, Hess Rise (100 Ma); M, Magellan Rise (135 Ma); MP, Mid-Pacific Mountains (tentatively assumed to have formed as early as 140 Ma; Madrigal et al., 2016); N, Nauru Basin (111 Ma); OJ, Ontong Java Nui (123 Ma); S, Shatsky Rise (144 Ma).

Plate with magma transported southwestward along the base of the lithosphere with the Tamu Massif erupting into an already relocated triple junction (Figure 10f) or alternatively impinged the lithosphere directly beneath southern Shatsky if the plume controlled the triple junction relocation between 150 and 144 Ma (Figures 10a and 10b; section 7). In both models, volcanic constructs may have covered all three plates; the Ori Massif was probably emplaced on the Izanagi Plate (Figure 10c), but most pieces were eventually transferred to the Pacific plate due to numerous northeastward directed ridge jumps. A hypothesized Shatsky Rise twin, however, may have traveled on the Farallon plate and collided with the North American margin in Late Cretaceous-Early Eocene times (e.g., Liu et al., 2010; Sigloch & Mihalynuk, 2013).

Most reconstructed LIPs of the past 300 Ma erupted near vertically above the surface-projected margins of the two antipodal Large Low Shear-wave Velocity Provinces (LLSVPs) in the lowermost mantle (e.g., Burke, 2011; Garnero et al., 2007; Torsvik et al., 2016), which we refer to as TUZO (beneath Africa) and JASON (beneath the Pacific). The margins of the LLSVPs, or plume generation zones (PGZs; Burke et al., 2008), are defined as the regions with the largest lateral shear wave velocity gradients in the lowermost mantle, directly above the core–mantle boundary (Torsvik et al., 2006). In the *s10mean* tomography model (Doubrovine et al., 2016) the PGZ is approximated by the 0.9% slow contour. Some (e.g., Austermann et al., 2014) argued that the observed correlation between the reconstructed LIPs and the margins of TUZO and JASON (e.g., Torsvik et al., 2016) can be equally well explained by plumes forming randomly over the entire LLSVP area, rather than by plumes from their margins. This criticism has been addressed by Doubrovine et al. (2016), who showed that probability models that assume plumes rising from the LLSVP margins provide the best fit for the distribution of reconstructed LIPs.

The Shatsky Rise, the Mid-Pacific Mountains, and Magellan Rise all erupted near vertically above the surface-projected eastern margin of JASON (Figures 15a and 15b). The Magellan Rise may have initially erupted on the Phoenix Plate (Figure 15b) but soon transferred to the Pacific plate after a ridge-jump (Figure 15c). Also, the plate polygon model of Matthews et al. (2016), that we largely follow, may be incorrect or Magellan Rise may be younger (≤133 Ma) than our assumed age of 135 Ma (Ernst et al., 2005, use an age of 145 Ma for the Magellan Rise).

During the Early Cretaceous (after 135 Ma) the Pacific plate drifted slowly westward with a small northerly component (Figure 14b), and the Ontong Java Nui erupted at around 123 Ma near vertically above the surface-projected southeast margin of JASON, an event which is considered to have led to the breakup of the Phoenix Plate into four new plates at ~120 Ma (Figure 15c). The Hess Rise erupted at around 100 Ma (Figure 15d) and shortly after that (perhaps around 95 Ma), the Pacific plate changed its course to a northwest direction.

In Figure 16 we have reconstructed the estimated plume eruption center for six Pacific LIPs (the Ontong Java, Manihiki, and Hikurangi LIPs are considered as fragments of a single LIP; the Ontong Java Nui). In Model R, the reconstructed plume centers plot on average 3.2 ± 2.8° from the PGZ of JASON (great-circle distance measured from the estimated plume center to the nearest point on the 0.9% slow contour). This value is lower than that obtained in the reconstructions using the WK08-A model (6.2 ± 4.2°).

7. Plume-Ridge Interactions and the Origin of the Shatsky Rise

LIPs activity affects plate tectonics by creating and modifying plate boundaries, as best exemplified among the Atlantic bordering continents. The opening of the Central Atlantic at ~195 Ma occurred shortly

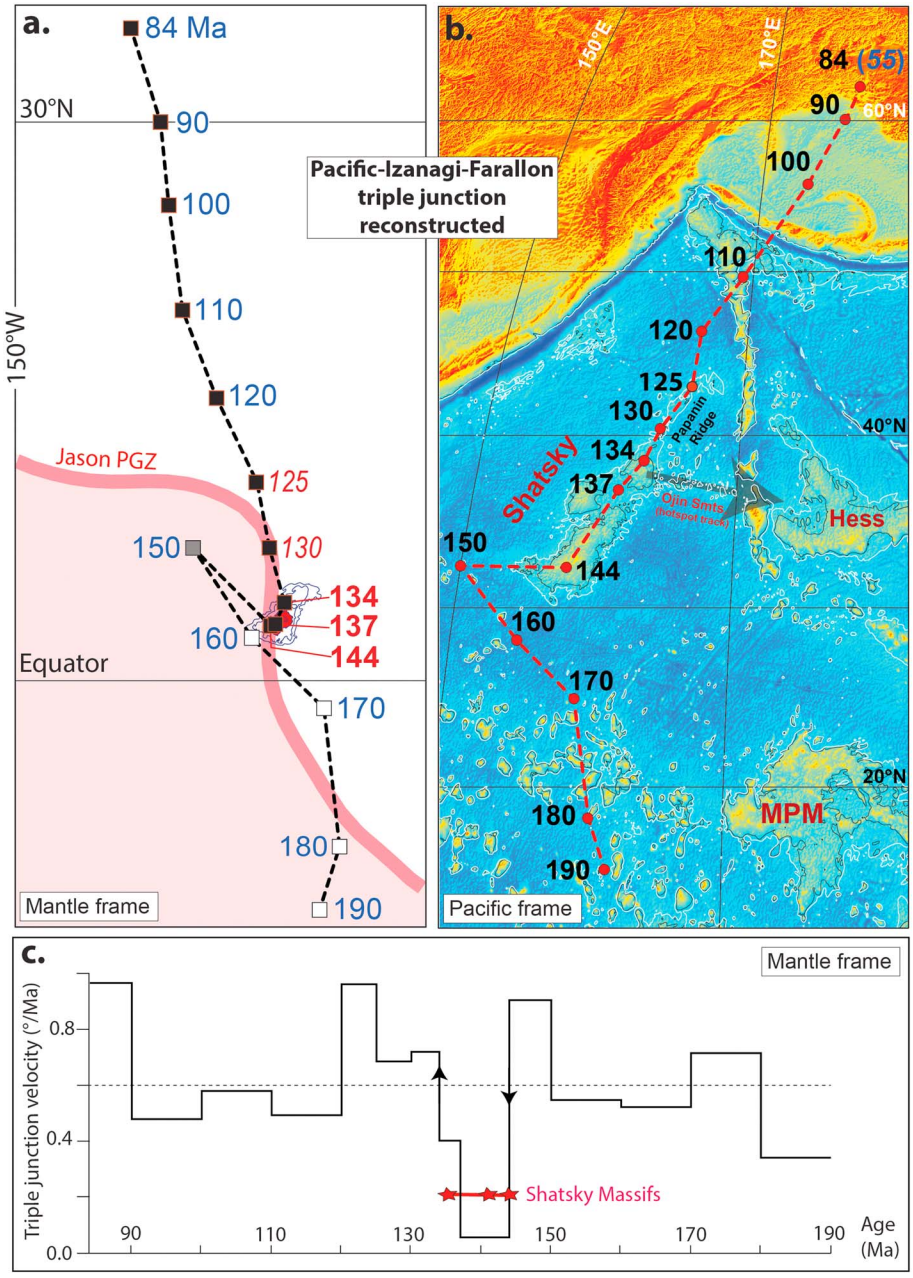

Figure 17. (a) Modeled motion of the Pacific-Izanagi-Farallon triple junction in a mantle frame. Based on GMHRF-3 extended with Model R from 83.5 to 150 Ma. We use modified dynamic plate polygons from Matthews et al. (2016). Before 150 Ma we use the plate rotation model of Matthews et al. (2016) where the Phoenix, Izanagi, and Farallon plates are reconstructed by plate circuits relative to a fixed Pacific plate back to 190 Ma. Because the Pacific plate in this model is not moving at all (only growing), the Pacific-Izanagi-Farallon triple junction is moving northward. Total cumulative great-circle motion from 190 Ma (birth of the Pacific plate) to 84 Ma (the demise of the Pacific-Izanagi-Farallon triple junction) is 63^{o} (~7,000 km). Note that the triple-junction started to be subducted around 55 Ma. Thick pink line is the JASON plume generation zone (PGZ). We show ≤4,000-m depth contours in southern Shatsky (blue thin lines) reconstructed to 144 Ma. Tamu Massif (south Shatsky) is shaded red. (b) Motion of the Pacific-Izanagi-Farallon triple junction (as in panel a) in present day coordinates (relative to Pacific plate). We plot 4,000 (highlighting the Shatsky Massifs and MPM; black lines) and 5,000 m (highlighting the Papanin Ridge and the Ojin Rise Seamounts: white lines) depth contours. Background image is ETOPO1. (c) Calculated triple junction velocities (mantle frame), averaging to about 0.6°/Ma. Note reduced velocities during the emplacement of the Shatsky Rise that may reflect that the triple junction was temporarily trapped above a relatively stable plume conduit.

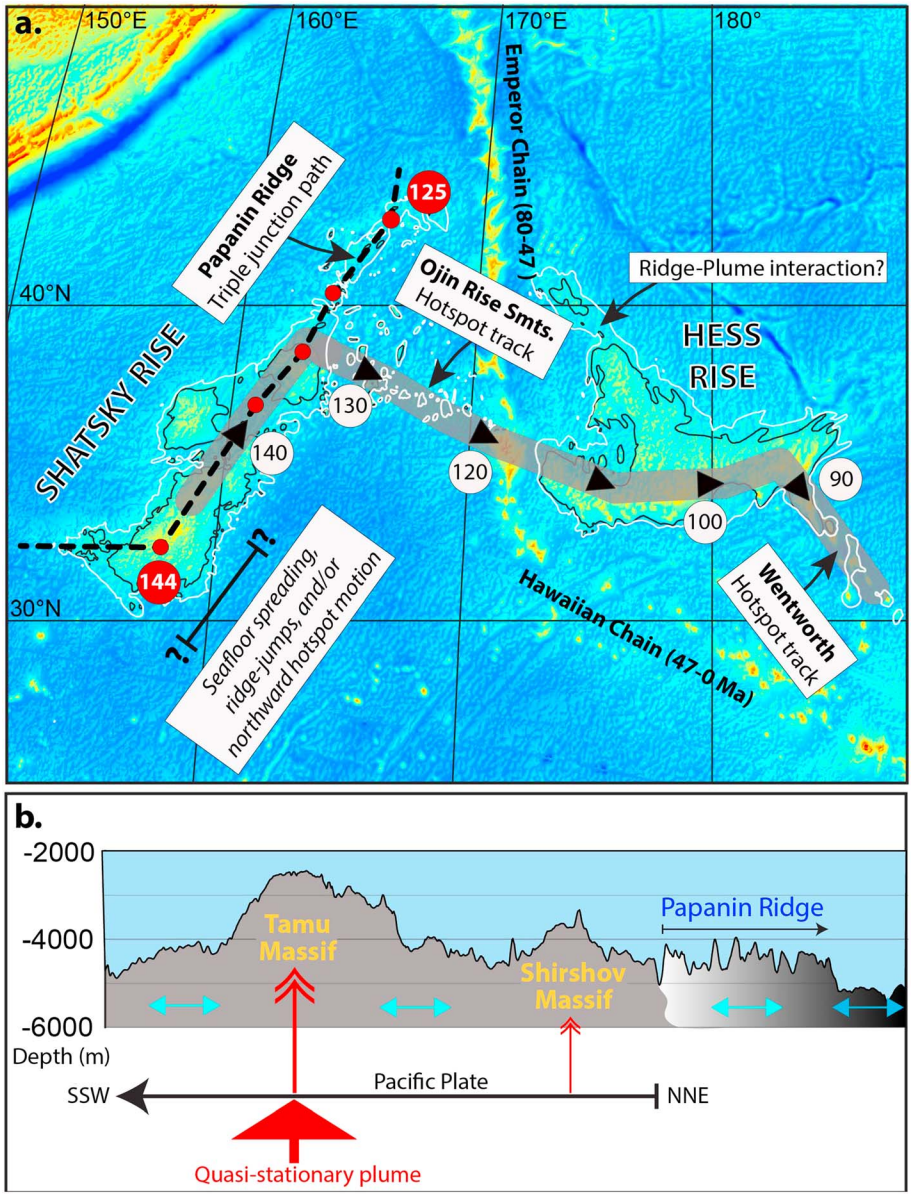

Figure 18. (a) Modeled Pacific plate motion (thick gray line) but made shorter along Shatsky Rise since clear evidence for ridge-plume interaction and seafloor spreading that will make Shatsky Rise longer (similar to Emperor). Also, ridge jump will make it longer since partly plume/seafloor will be relocated to the Pacific plate and possible northward hot spot drift can also make it longer; the real effect in kilometers will remain uncertain. Plate motion change at around 135 Ma following Ojin Rise seamounts (hot spot track), then a renewed phase of strong plume activity at Hess Rise time (~100 Ma) and then along Wentworth seamounts after 95 Ma. The Papanin Ridge is the track of the triple junction after 134 Ma, possibly including some upside-down drainage into the northward moving triple junction. No excess volcanism occurred in association with the triple junction after 125 Ma. (b) Bathymetry along the black d triple-junction path in panel a. The main Shatsky Rise (strong plume influence) in this profile is characterized by the Tamu and Shirshov Massifs (reaching minimum water depths of about 2,500 m at TAMU), the Papanin Ridge is characterized by short wave length seamounts located at 4,000-m depths or more, while after 125 Ma, a flattish seafloor is observed (about 5,000-m water depth).

after the emplacement of the Central Atlantic Magmatic Province (201 Ma). Then the Paraná-Etendeka (134 Ma) heralded the early opening of the South Atlantic (~130 Ma), and finally, the North Atlantic Igneous Province (NAIP; starting at 62 Ma) assisted the opening of the Northeast Atlantic at around 54–55 Ma (Buiter & Torsvik, 2014; Svensen et al., 2017; Torsvik & Cocks, 2017, 2013). At many margins,

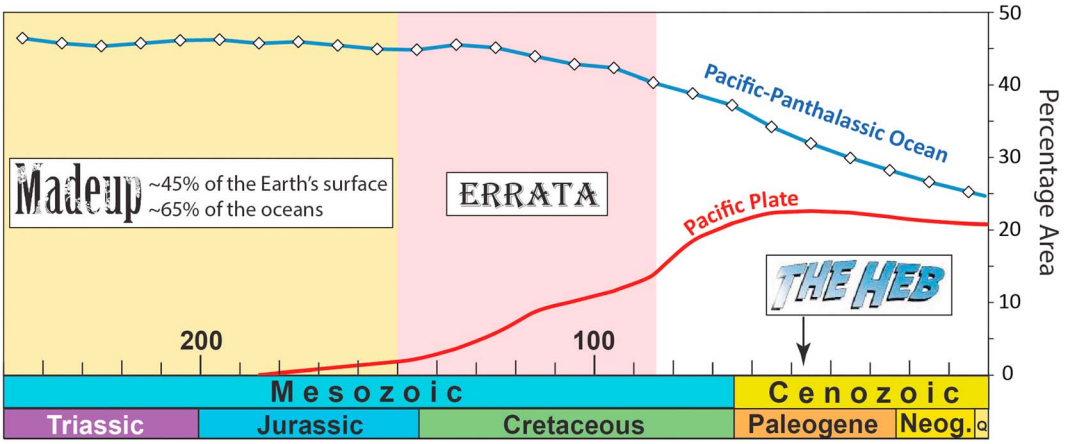

Figure 19. Size of the Pacific-Panthalassic Ocean Basin (all the oceanic plates) for the past 250 Myrs and the size of the Pacific plate since its inception at around 190 Ma. Sizes are the percentage of the total Earth surface through time. After 83.5 Ma the Pacific Ocean plates are reconstructed with a global moving hot spot reference frame. Pacific-Panthalassic reconstructions can only be extended from 83.5 Ma to ~144 Ma (Shatsky Rise) using a combination of a fixed hot spot frame and true polar wander corrected paleomagnetic data (see text). Before that time, there are no absolute reference frames that can relate the Panthalassic plates to the mantle or the spin axis and thus ~45% of the Earth's surface (65% of the oceanic areas) cannot be reconstructed in an absolute sense before 144 Ma (extrapolated to 150 Ma; Table 4). This, combined with largely flawed plate reconstructions between 144 and 83.5 Ma and continuous debates concerning the Cenozoic origin of the Hawaiian-Emperor Bend (HEB) renders Pacific-Panthalassic reconstructions challenging.

rifting began before the main phase of LIP volcanism, which suggests that rifting was initiated by tectonic forces and that mantle plume material was guided toward the thinned rifted lithosphere to help trigger final continental breakup (e.g., Buiter & Torsvik, 2014). Plumes impinging the oceanic lithosphere also influence the configuration of plates, for example, by relocating plate boundaries (ridge jumps) or making entirely new plates. As an example, the eruption of the ~123 Ma Ontong Java Nui may have led to the breakup of the Phoenix Plate into four new plates at ~120 Ma (Figure 15c).

The northwest Pacific M-sequence (Japanese) lineations (Figures 10b and 10c) show a clear change in spreading direction and a triple junction relocation at around M20 time. Using the time scale of Gee and Kent (2007) this reorganization occurred between 144.7 and 143.36 Ma, thus overlapping with the emplacement ages of the Tamu Massif. Conversely, using the time scale of Ogg (2012), the Chron M20 reorganization would have occurred at 147.72–146.54 Ma, shortly before the construction of the Tamu Massif. To explore this issue further we have analyzed the Pacific-Izanagi-Farallon triple junction (PIFTJ) in space and time for both mantle and Pacific (in situ) reference frames (Figures 17 and 18).

Triple junctions are *stable geometrical* configurations but the PIFTJ has moved almost 7,000 km northward since its inception, shortly after 190 Ma, to its demise at ~84 Ma (Figure 17a). PIFTJ reconstructions are most reliable since 144 Ma, the 150 Ma reconstruction is extrapolated, and before that time, there is no way to reconstruct the triple junction in an absolute sense. In the *Earthbyte* model (e.g., Matthews et al., 2016) the Pacific plate is fixed with respect to the mantle between 190 and 150 Ma, and the PIFTJ moves because of a steadily growing Pacific plate. This is a speculative and subjective model ("Made-up" in Figure 19a), originally suggested by Engebretson et al. (1985) for the period between 180 and 145 Ma. Taken at face value, however, and with a lack of objective alternatives, the triple junction moved northward until 150 Ma. It then shifted southeastward in the mantle frame (Figure 17a), and the initial Shatsky Rise volcanism (Tamu Massif) and the PIFTJ coincide, and importantly, overlie the PGZ of JASON at 144 Ma. In its lifetime, the PIFTJ was only associated with excessive volcanism between 144 and 134 Ma (continuing to 125 Ma with much less excess volcanism along the Papanin Ridge, Figure 17b), when the triple junction was located near-vertically above the surface projection of PGZ of JASON (Figure 17a). The PIFTJ was moving at a speed of about 0.6°/Ma between 190 and 84 Ma, but during peak Shatsky magmatism the velocity was much reduced (Figure 17c), and the cumulative motion of the PIFTJ with respect to the mantle amounts to only 175 km between 144 and 134 Ma. Conversely, the jump of the triple-junction between 150 and 144 Ma was about 800 km (Figures 10b, 10d, and 18b). Our analysis suggests that the initial emplacement of the Shatsky Rise LIP led to the jump of the PIFTJ: Subsequent PIFTJ changes from 144 Ma, and onward,

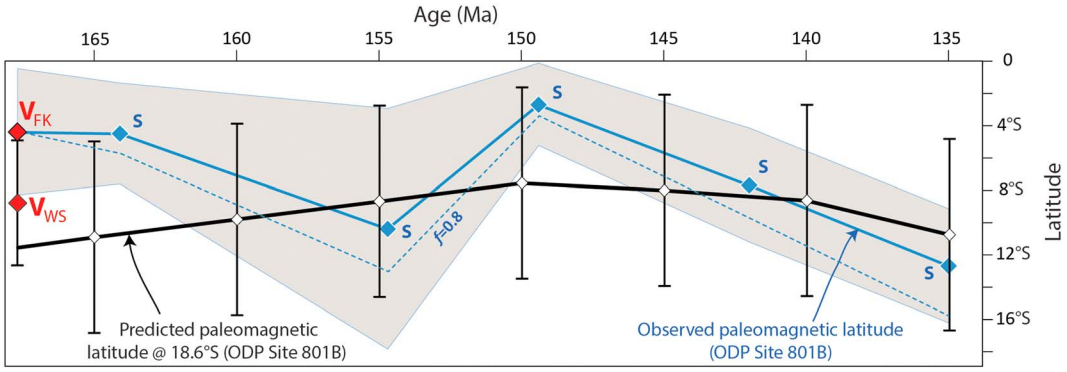

Figure 20. Paleolatitudes from the Pacific plate (ODP Site 801B) derived from paleomagnetic data from sedimentary rocks (marked S) and one volcanic site (marked V_{FK}) at ~167.7 Ma (Fu & Kent, 2018). Another dip-corrected volcanic latitude estimate from ODP Site 801C (Wallick & Steiner, 1992) has a slightly higher southerly latitude and marked V_{WS}. We also show paleomagnetic latitudinal estimates after considering that the sedimentary rocks may have been affected by very minor inclination shallowing effects ($f = 0.8$). Latitude estimates in Fu and Kent (2018) were reported with 1σ errors and the gray-shaded regions represent the area of 95% confidence (1.96σ). For comparison we show the predicted paleomagnetic latitudes from our Model R; we have assigned a nominal latitude uncertainty of 3° (1σ), and error bars are shown at the 95% confidence level.

were controlled by the quasi-stationary Shatsky plume location with the Pacific plate moving in a southwestward direction until about 135 Ma. After that time, the Ojin Rise Seamounts tracked the Pacific plate while the PIFTJ moved along the Papanin Ridge with possibly some upside-down drainage from the Shatsky plume. After 125 Ma the PIFTJ was not associated with abnormal volcanic production, at least until around 110 Ma (the seafloor associated with the PIFTJ history younger than ~108 Ma has been subducted, starting at around 55 Ma; Figure 17b).

8. Concluding Remarks and the Way Forward

Reconstruction of the time-dependent mosaic of plates that comprised the Pacific-Panthalassic oceans is of paramount importance because that massive oceanic domain represented 25–45% of the Earth's surface (Figure 19)—and housed the main subduction factories on our Mesozoic-Cenozoic planet. We have here documented that two prominent Pacific-Panthalassic plate models (83.5–150 Ma) are variably flawed. In the first model (Steinberger & Gaina, 2007) the Pacific plate is rotated 9° compared with the corrected model at 150 Ma (Figure 7a). The corrected model (section 4.1, Erratum 1) leads to increased net lithosphere rotation (NR) and thus NR calculated in Torsvik et al. (2010) should be adjusted between 150 and 90 Ma (Table 2). The second incorrect Pacific model (section 4.2, Erratum 2) is more worrying: This model is used and incorporated in all public releases of the widely used GPlates application (e.g., Matthews et al., 2016; GPlates release 2.0/2.1), and yields a Pacific plate reconstruction that is rotated by as much as 39° with respect to the corrected orientation of the Pacific plate at 150 Ma (Figure 7b). Since most other plates in the Panthalassic Ocean are linked through relative plate circuits to the Pacific plate, the erroneous Pacific plate model affects the entire Pacific-Panthalassic Ocean and its connections to all surrounding active margins. To rectify this, we could simply have implemented the Wessel and Kroenke (2008) model correctly within the faulty *Earthbyte* model (Table 3), but the corrected model implies high Pacific plate angular velocities and high NR (Figure 13).

Because of the high Pacific plate velocities and NR due to the entire Pacific-Panthalassic Basin rotating systematically clockwise before 83.5 Ma (Figure 8b *inset* diagram) in the Wessel and Kroenke (2008) model, we opted to devise new absolute Pacific plate models between 83.5 and 150 Ma. Our simplest model (Model S) connects the Shatsky and Hess Rises in a rather direct manner and resembles the model of Duncan and Clague (1985) but with lower NR. Model R (refined) assumes that at least parts of the northeast trend of volcanism for Shatsky Rise (~144–135 Ma) is a real hot spot track while reproducing the (curved) Mid-Pacific Mountains and the (linear) Wentworth and Musicians Chains. Model R is our preferred model; modeled paleomagnetic latitudes fit well with the observations, and both NR and Pacific plate velocities are low (Figure 13). Pacific LIPs, when reconstructed, are located near vertically above the surface-projected

margin of the JASON LLSVP (Figure 16), a correlation noticed for LIPs linked to the TUZO LLSVP for the past 300 Ma (e.g., Doubrovine et al., 2016; Torsvik et al., 2016).

The Shatsky volcanic centers (Tamu, Ori, and Shirshov; Figure 9a) can be related to a quasi-stationary plume that controlled the location of the Pacific-Izanagi-Farallon triple junction. Motion of the triple junction between 144 and 134 Ma can be modeled as northward hot spot drift or northward ridge jump and thus lengthening the Shatsky Rise by about 175 km. Vigorous seafloor spreading and mid-ocean ridge-hot spot interactions within vast parts of the Shatsky Rise have been also postulated by Huang et al. (2018), based on interpretations of a new magnetic anomaly map.

Incidentally, the flawed *Earthbyte* model is a somewhat better match with Model R than the corrected *Earthbyte* model and the original model of Wessel and Kroenke (2008); this is *fortuitously* good news, since the flawed *Earthbyte* model (GPlates default) has been used for most Mesozoic full-plate tectonic reconstructions and geodynamic exercises. Conversely, implementing the Wessel and Kroenke (2008) model correctly within the *Earthbyte* model would necessitate radical revision of countless studies, but also require a redesign of the 250–150 Ma model. However, there are few direct observations to reconstruct the Panthalassic plates in an absolute sense before 150 Ma ("Madeup" in Figure 19). We must therefore rely on plate tectonic principles, continental margin geology and the identification of intraoceanic subducted slabs from seismic tomography (e.g., Domeier et al., 2016; Shephard et al., 2017; Sigloch & Mihalynuk, 2013; van der Meer et al., 2010, 2012, 2017) to tentatively reconstruct the former plate boundaries and restore the lost oceanic lithosphere.

For reasons stated in section 5, we have only used paleomagnetic data from volcanic rocks to calibrate our new Pacific plate models, but in Figure 20 we compare the predicted paleomagnetic latitude for Model R with paleomagnetic observations from sedimentary rocks from ODP Site 801B (Fu & Kent, 2018). Our model R is extrapolated back to 150 Ma and the predicted paleomagnetic latitudes are statistically overlapping (95% confidence level) with those derived from the sedimentary-based paleomagnetic data, despite potential inclination shallowing effects that bias derived latitudes toward erroneously low values. Before 150 Ma, our model (Appendix A) simply follows the *Earthbyte* procedure (e.g., Matthews et al., 2016; Müller et al., 2016) of keeping the Pacific plate at a constant latitude with respect to the mantle frame ("Madeup" in Figure 19), but we notice that predicted paleomagnetic latitudes (which differ from the mantle frame because of TPW) overlap with ODP Site 801B sedimentary results back to about 165 Ma (Figure 20). Importantly, Fu and Kent (2018) also reported paleomagnetic results from the oldest igneous rocks recovered from the Pacific plate, which yielded a latitude estimate of about 4.4°S at ~167.7 Ma. This result is still overlapping with our Model R estimates, but can potentially be used to position the Pacific plate at a slightly lower southerly latitude in the Middle Jurassic. If we reposition the Pacific plate as such, the latitudes in the mantle frame would also be lower (~6°), and in that frame the Pacific plate would then show a component of southerly movement from about 170 to 135 Ma, before changing its course to a northwesterly direction (Figure 14a).

Intuitively, one may think that the youngest history of the Pacific Basin (after 83.5 Ma) should be relatively straightforward to agree upon—but unfortunately not. This largely stems from the fact that the origin of the Hawaiian-Emperor Bend (HEB; Figures 5 and 19) continues to be debated (e.g., Finlayson et al., 2018; Tarduno & Bono, 2019). Some still argue that rapid southward drift of the Hawaiian hot spot before 47 Ma is all that is needed to explain the bend (e.g., Tarduno & Koppers, 2019), but this simply does not work geometrically (Torsvik et al., 2017), and all published GMHRF's (i.e., Doubrovine et al., 2012; Steinberger et al., 2004; Torsvik et al., 2008), or modifications of these (e.g., Matthews et al., 2016; Müller et al., 2016), model the HEB as a plate motion change (Figure 5).

Appendix A: Description of Accompanying GPlates Files

Two data files (PACIFIC.ZIP and Pacific_EARTHBYTE_Model_R.ZIP) can be downloaded from http://www.earthdynamics.org/Pacific/PACIFIC.zip and http://www.earthdynamics.org/Pacific/Pacific_EARTHBYTE_Model_R.zip.

These files can also be downloaded at www.earthdynamics.org/earthmodel.

PACIFIC.ZIP

The following files are included:

1. *Global_Model_R.gproj* (GPlates project file that will load all files below).
2. *Global_Model_R.rot* (GPlates rotation file 0–250 Ma; modified from Matthews et al., 2016).
3. *Global_Model_R.gpml* (GPlates Dynamic plate polygon model; modified from Matthews et al., 2016.
4. *Pacific_LIPS.gpml* (Pacific LIP polygons used in this paper).
5. *PGZ_s10mean.gpml* (Plume generation zones; s10mean 0.9% slow contour; Doubrovine et al., 2016).
6. *s10mean.63.2800.gpml* (s10mean grid model at 2800 km depth; Doubrovine et al., 2016).
7. *tomoTHT.cpt* (grid color palette used with s10mean model).

Rotation File (Global_Model_R.ROT)

Our plate reconstructions in GPlates format use a hybrid plate motion frame that combines hot spot and TPW corrected paleomagnetic (before 125 Ma) reference frames, which can be referred to as a mantle frame (e.g., Doubrovine et al., 2016). The original rotation file is that of Matthews et al. (2016; GPlates 2.0 default), but modifications include (i) the revised Pacific extension from 83.5 to 150 Ma (Model R developed here), (ii) critical plate circuits adjusted to conform with GMHRF-3 (Doubrovine et al., 2012) and those used to develop the global apparent polar wander path in Torsvik et al. (2012), and (iii) implementation of a switch between the mantle (Plate Id. = 0) and paleomagnetic (Plate Id. = 1) reference frames.

Adjusted rotations are marked with "CEED" in the right-hand comment/information column, the rotation file works back to 250 Ma, and can be used to reconstruct all other files supplied with GPlates 2.0/2.1 (e.g., magnetic isochrones, coastlines). The rotation file does not work satisfactorily with continents and terranes published in Torsvik and Cocks (2017) due to some differing plate identification numbers.

At start-up, the GPlates software defaults to a mantle frame (Plate Id = 0). In order to show our reconstructions with respect to the spin axis (paleomagnetic or paleogeographic frame), select option "Reconstruction," suboption "Specify Anchored Plate ID," and replace "0" with "1."

Plate reconstructions that aim to explore paleoclimate (e.g., plotting latitudinal sensitive sedimentary facies) or comparing reconstructions with global climate simulations or other paleomagnetic reconstructions should always be reconstructed with Plate Id = 1. Conversely, Plate Id = 0 (mantle frame) should be used as input for mantle modeling and, for example, to compare surface volcanism such as large igneous provinces with deep mantle anomalies (Figure 16) or mantle slabs with surface locations of subduction. The enclosed file "PGZ_s10mean.gpml" (plume generation zones) is coded such that it is also possible to relate deep mantle processes to surface processes in the palaeomagnetic reference frame because the plume generation zones (PGZs) will be rotated according to the amount of true polar wander at a specific reconstruction time. In this neat way, one can perceive how the surface distribution of, for example, large igneous provinces and kimberlites relate to the deep mantle, and at the same time plot climatically sensitive sedimentary data that should not be corrected for true polar wander (see Torsvik & Cocks, 2017)

Dynamic Plate Polygon Model (Global_Model_R.gplm)

GPlates allows full-plate model construction using time-dependent plate boundaries which self-close at any arbitrary spatial or temporal scale to form dynamic polygons (Gurnis et al., 2012). The original model is that of Seton et al. (2012), developed back to 200 Ma. Here we use the model of Matthews et al. (2016) back to 250 Ma (the default of GPlates 2.0), but because we have revised critical plate circuits and rotation poles (including a new Model R for the Pacific), the polygon model required many modifications to close the polygons appropriately (mostly working satisfactory). We have not added new plates or otherwise implemented radical changes to the original plate polygon model.

Pacific_EARTHBYTE_Model_R.ZIP

This file includes *EARTHBYTE_Model_R.gproj* that will load the following files:

1. *EARTHBYTE_Rotation_Model_R.rot* (GPlates rotation file 0-250 Ma).
2. *EARTHBYTE_Plate_Model_R.gpml* (GPlates Dynamic plate polygon model).

The two files are the original files of Matthews et al. (2016; default GPlates 2.0), but the rotation file has been adapted to our Pacific Model R, which also required changes in the dynamic plate polygon model.

Acknowledgments

This work was supported by the Research Council of Norway (RCN), through its Centres of Excellence funding scheme, project 223272 (CEED), through RCN project 250111 (600 Myr Plate Model) to M. D., and through RCN project 274085 (Changing Continents, Climates and Sea Levels) to T. H. T. (sabbatical Potsdam 2018). B. S. thanks Kevin Konrad for pointing out inconsistencies that are corrected in Erratum 1. We also thank Roger Fu and an anonymous reviewer for constructive comments. GPlates compatible rotation and data files available at http://www.earthdynamics.org/earth-model/index.html see (Appendix A).

References

Amante, C. & Eakins, B.W. (2009). ETOPO1 1 Arc-minute global relief model: Procedures, data sources and analysis. NOAA Technical Memorandum NESDIS, NGDC-24, 19 pp.

Austermann, J., Kaye, B. T., Mitrovica, J. X., & Huybers, P. (2014). A statistical analysis of the correlation between large igneous provinces and lower mantle seismic structure. *Geophysical Journal International*, *197*(1), 1–9. https://doi.org/10.1093/gji/ggt500

Becker, T., Schaeffer, A., Lebedev, S., & Conrad, C. P. (2015). Toward a generalized plate motion reference frame. *Geophysical Research Letters*, *42*, 3188–3196. https://doi.org/10.1002/2015GL063695

Bercovici, D., & Mahoney, J. (1994). Double flood basalts and plume head separation at the 660-kilometer discontinuity. *Science*, *266*(5189), 1367–1369. https://doi.org/10.1126/science.266.5189.1367

Bilardello, D., & Kodama, K. P. (2010a). Paleomagnetism and magnetic anisotropy of Carboniferous red beds from the Maritime Provinces of Canada: Evidence for shallow paleomagnetic inclinations and implications for North American apparent polar wander. *Geophysical Journal International*, *180*(3), 1013–1029. https://doi.org/10.1111/j.1365-246X.2009.04457.x

Bilardello, D., & Kodama, K. P. (2010b). Rock magnetic evidence for inclination shallowing in the early Carboniferous Deer Lake group red beds of western Newfoundland. *Geophysical Journal International*, *181*(1), 275–289. https://doi.org/10.1111/j.1365-246X.2010.04537.x

Bryan, S. E., Peate, I. U., Peate, D. W., Jerram, D. A., Mawby, M. R., Marsh, J. S., & Miller, J. A. (2010). The largest volcanic eruptions on Earth. *Earth-Science Reviews*, *102*(3-4), 207–229. https://doi.org/10.1016/j.earscirev.2010.07.001

Buiter, S. J. H., & Torsvik, T. H. (2014). A review of Wilson Cycle plate margins. *Gondwana Research*, *26*(2), 627–653. https://doi.org/10.1016/j.gr.2014.02.007

Burke, K. (2011). Plate tectonics, the Wilson Cycle, and mantle plumes: Geodynamics from the top. *Annual Review of Earth and Planetary Sciences*, *39*(1), 1–29. https://doi.org/10.1146/annurev-earth-040809-152521

Burke, K., Steinberger, B., Torsvik, T. H., & Smethurst, M. A. (2008). Plume generation zones at the margins of large low shear velocity provinces on the core–mantle boundary. *Earth and Planetary Science Letters*, *265*(1-2), 49–60. https://doi.org/10.1016/j.epsl.2007.09.042

Burke, K., & Torsvik, T. H. (2004). Derivation of large igneous provinces of the past 200 million years from long-term heterogeneities in the deep mantle. *Earth and Planetary Science Letters*, *227*(3-4), 531–538. https://doi.org/10.1016/j.epsl.2004.09.15

Chandler, M. T., Wessel, P., Taylor, B., Seton, M., Kim, S.-S., & Hyeong, K. (2012). Reconstructing Ontong Java Nui: Implications for Pacific absolute plate motion, hot spot drift and true polar wander. *Earth and Planetary Science Letters*, *331-332*, 140–151. https://doi.org/10.1016/j.epsl.2012.03.017

Chen, S., & Liu, J. (2018). Geochemical characteristic and geological significance of Cretaceous phonotephrite from the Mid-Pacific Mountains. *Science China Earth Sciences*, *61*(6), 745–764. https://doi.org/10.1007/s11430-017-9172-4

Clouard, V., & Bonneville, A. (2005). Ages of seamounts, islands and plateaus on the Pacific plate. In G. Foulger, et al. (Eds.), *Plates, plumes, and paradigms*, *Special Paper*, (Vol. 388, pp. 71–90). Boulder, Colorado: Geological Society of America.

Coffin, M. F., & Eldholm, O. (1994). Large igneous provinces: Crustal structure, dimensions, and external consequences. *Reviews of Geophysics*, *32*(1), 1–36. https://doi.org/10.1029/93RG02508

Conrad, C. P., Steinberger, B., & Torsvik, T. H. (2013). Stability of active mantle upwelling revealed by net characteristics of plate tectonics. *Nature*, *498*(7455), 479–482. https://doi.org/10.1038/nature12203

Cox, A., & Gordon, R. G. (1984). Paleolatitudes determined from palaeomagnetic data from vertical cores. *Reviews Geophysical Space Physics*, *22*(1), 47–72. https://doi.org/10.1029/RG022i001p00047

Cox, A., & Hart, R. (1986). *Plate tectonics: How it works*, (p. 392). Malden, Massachussetts: Blackwell Science.

Domeier, M., Doubrovine, P. V., Torsvik, T. H., Spakman, W., & Bull, A. L. (2016). Global correlation of lower mantle structure and past subduction. *Geophysical Research Letters*, *43*, 4945–4953. https://doi.org/10.1002/2016GL068827

Domeier, M., Van der Voo, R., & Torsvik, T. H. (2012). Paleomagnetism and Pangea: The road to reconciliation. *Tectonophysics*, *514*, 14–43.

Doubrovine, P. V., Steinberger, B., & Torsvik, T. H. (2012). Absolute plate motions in a reference frame defined by moving hot spots in the Pacific, Atlantic and Indian oceans. *Journal Geophysical Research*, *117*, B09101. https://doi.org/10.1029/2011JB009072

Doubrovine, P. V., Steinberger, B., & Torsvik, T. H. (2016). A failure to reject: Testing the correlation between large igneous provinces and deep mantle structures with EDF statistics. *Geochemical Geophysics Geosystems*, *17*, 1130–1163. https://doi.org/10.1002/2015GC006044

Duncan, R. A., & Clague, D. A. (1985). Pacific plate motion recorded by linear volcanic chains. In A. E. M. Nairn, F. G. Stehli, & S. Uyeda (Eds.), *The Ocean Basins and Margins: The Pacific Ocean*, (Vol. 7a, pp. 89–121). New York: Plenum.

Eldholm, O., & Coffin, M. F. (2000). Large igneous provinces and plate tectonics. In M. A. Richards, R. G. Gordon, & R. D. van der Hilst (Eds.), *The history and dynamics of global plate motions*, (pp. 309–326). Washington, D.C: American Geophysical Union. https://doi.org/10.1029/GM121p0309

Engebretson, D. C., Cox, A., & Gordon, R. G. (1985). *Relative motions between oceanic and continental plates in the Pacific Basin*, *Special Paper*, (Vol. 206, p. 59). Boulder, Colorado: Geological Society America.

Ernst, R. E. (2014). *Large igneous provinces*. London: Cambridge University Press. https://doi.org/10.1017/CBO9781139025300

Ernst, R. E., Buchan, K. L., & Campbell, I. H. (2005). Frontiers in large igneous province research. *Lithos*, *79*(3-4), 271–297. https://doi.org/10.1016/j.lithos.2004.09.004

Fiet, N., Quidelleur, X., Parize, O., Bulot, L. G., & Gillot, P. Y. (2006). Lower Cretaceous stage durations combining radiometric data and orbital chronology: Toward a more stable relative time scale? *Earth and Planetary Science Letters*, *246*(3-4), 407–417. https://doi.org/10.1016/j.epsl.2006.04.014

Finlayson, V. A., Konter, J. G., Konrad, K., Koppers, A. A. P., Jackson, M. G., & Rooney, T. O. (2018). Sr–Pb–Nd–Hf isotopes and $^{40}Ar/^{39}Ar$ ages reveal a Hawaii–Emperor-style bend in the Rurutu hotspot. *Earth and Planetary Science Letters*, *500*, 168–179. https://doi.org/10.1016/j.epsl.2018.08.020

French, S. W., & Romanowicz, B. A. (2015). Broad plumes rooted at the base of the Earth's mantle beneath major hotspots. *Nature*, *525*, 95–99.

Fu, R. R., & Kent, D. V. (2018). Anomalous Late Jurassic motion of the Pacific plate with implications for true polar wander. *Earth and Planetary Science Letters*, *490*, 20–30. https://doi.org/10.1016/j.epsl.2018.02.034

Garnero, E. J., Lay, T., & McNamara, A. (2007). *Implications of lower mantle structural heterogeneity for existence and nature of whole mantle plumes*, *Special Paper*, (Vol. 430, pp. 79–102). Boulder, Colorado: Geological Society America.

Gee, J. S., & Kent, D. V. (2007). Source of oceanic magnetic anomalies and the geomagnetic polarity time scale. In *Treatise on Geophysics, Vol. 5: Geomagnetism* (pp. 455–507). Amsterdam: Elsevier.

Geldmacher, J., Van den Bogaard, P., Heydolph, K., & Hoernle, K. (2014). The age of Earth's largest volcano: Tamu Massif on Shatsky Rise (northwest Pacific Ocean). *International Journal Earth Sciences (Geol. Rundsch.)*, *103*(8), 2351–2357. https://doi.org/10.1007/s00531-014-1078-6

Granot, R., Cande, S. C., Stock, J. M., & Damaske, D. (2013). Revised Eocene-Oligocene kinematics for the West Antarctic rift system. *Geophysical Research Letters*, *40*, 279–284. https://doi.org/10.1029/2012GL054181

Gripp, A., & Gordon, R. G. (2002). Young tracks of hotspots and current plate velocities. *Geophysical Journal International*, *150*(2), 321–361. https://doi.org/10.1046/j.1365-246X.2002.01627.x

Gurnis, M., Turner, M., Zahirovic, S., DiCaprio, L., Spasojevic, S., Müller, R. D., et al. (2012). Plate tectonic reconstructions with continuously closing plates. *Computers & Geosciences*, *38*(1), 35–42.

He, H., Pan, Y., Tauxe, L., Qin, H., & Zhu, R. (2008). Toward age determination of the M0r (Barremian-Aptian boundary) of the Early Cretaceous. *Physics of the Earth and Planetary Interiors*, *169*(1-4), 41–48. https://doi.org/10.1016/j.pepi.2008.07.014

Heaton D.E. & Koppers A.A.P. (2014) Constraining the rapid construction of TAMU Massif at an 145 Myr old triple junction, Shatsky Rise. Annual V. M. In Goldschmidt Conference (abstr.) # 948.

Huang, Y., Sager, W. W., Tominaga, M., Greene, J. A., Zhang, J., & Nakanishi, M. (2018). Magnetic anomaly map of Ori Massif and its implications for oceanic plateau formation. *Earth and Planetary Science Letters*, *501*, 46–55. https://doi.org/10.1016/j.epsl.2018.08.029

Kent, D. V., & Tauxe, L. (2005). Corrected Late Triassic latitudes for continents adjacent to the North Atlantic. *Science*, *307*(5707), 240–244. https://doi.org/10.1126/science.1105826

Kodama, K. P. (2009). Simplification of the anisotropy-based inclination correction technique for magnetite- and hematite bearing rocks: A case study for the Carboniferous Glenshaw and Mauch Chunk formations, North America. *Geophysical Journal International*, *176*(2), 467–477. https://doi.org/10.1111/j.1365-246X.2008.04013.x

Koppers, A. A. P. (2010). Massive basalt flows on the southern flank of Tamu Massif, Shatsky Rise: A reappraisal of ODP Site 1213 basement units. In W. Sager, T. Sano, J. Geldmacher, et al. (Eds.), *Proceedings of the Integrated Ocean Drilling Program*, (Vol. 324, 20 pp.). Tokyo: IODP. https://doi.org/10.2204/iodp.proc.324.2010

Liu, L., Gurnis, M., Seton, M., Saleeby, J., Müller, R. D., & Jackson, J. M. (2010). The role of oceanic plateau subduction in the Laramide orogeny. *Nature Geosciences*, *3*(5), 353–357. https://doi.org/10.1038/ngeo829

Madrigal, P., Gazel, E., Flores, K., Bizimis, M., & Jicha, B. (2016). Record of massive upwellings from the Pacific large low shear velocity province. *Nature Communications*, *7*(1), 13309. https://doi.org/10.1038/ncomms13309

Mahoney, J. J., Duncan, R. A., Tejada, M. L. G., Sager, W. W., & Bralower, T. J. (2005). Jurassic-Cretaceous boundary age and mid-ocean-ridge-type mantle source for Shatsky Rise. *Geology*, *33*(3), 185–188. https://doi.org/10.1130/G21378.1

Malinverno, A., Hildebrandt, J., Tominaga, M., & Channell, J. E. T. (2012). M-sequence geomagnetic polarity time scale (MHTC12) that steadies global spreading rates and incorporates astrochronology constraints. *Journal Geophysical Research*, *117*, B06104. https://doi.org/10.1029/2012JB009260

Matthews, K., Maloney, K. T., Zahirovic, S., Williams, S. E., Seton, M., & Müller, R. D. (2016). Global plate boundary evolution and kinematics since the late Paleozoic. *Global and Planetary Change*, *146*, 226–250. https://doi.org/10.1016/j.gloplacha.2016.10.002

Midtkandal, I., Svensen, H. H., Planke, S., Corfu, F., Polteau, S., Torsvik, T. H., et al. (2016). The Aptian (Early Cretaceous) oceanic anoxic event (OAE1a) in Svalbard, Barents Sea, and the absolute age of the Barremian-Aptian boundary. *Palaeogeography, Palaeoclimatology, Palaeoecology*, *463*, 126–135. https://doi.org/10.1016/j.palaeo.2016.09.023

Mittelstaedt, E., Ito, G., & van Hunen, J. (2011). Repeat ridge jumps associated with plume-ridge interaction, melt transport, and ridge migration. *Journal Geophysical Research*, *116*, B01102. https://doi.org/10.1029/2010JB007504

Molnar, P., & Stock, J. (1987). Relative motions of hotspots in the Pacific, Atlantic and Indian Ocean since late Cretaceous time. *Nature*, *327*(6123), 587–591. https://doi.org/10.1038/327587a0

Morgan, W. J. (1972a). Plate motions and deep mantle convection. *Geological Society America Memoir*, *132*, 7–22. https://doi.org/10.1130/MEM132-p7

Morgan, W. J. (1972b). Deep mantle convection plumes and plate motions. *AAPG Bulletin*, *56*, 203–213.

Müller, R. D., Royer, J.-Y., & Lawver, L. A. (1993). Revised plate motions relative to the hotspots from combined Atlantic and Indian Ocean hotspot tracks. *Geology*, *21*(3), 275–278. https://doi.org/10.1130/0091-7613(1993)021<0275:RPMRTT>2.3.CO;2

Müller, R. D., Seton, M., Zahirovic, S., Williams, S. E., Matthews, K. J., Wright, N. M., et al. (2016). Ocean basin evolution and global-scale plate reorganization events since Pangea breakup. *Annual Reviews Earth and Planetary Science*, *44*(1), 107–138. https://doi.org/10.1146/annurev-earth-060115-012211

Nakanishi, M., Sager, W. W., & Klaus, A. (1999). Magnetic lineations within Shatsky Rise, northwest Pacific Ocean: Implications for hot spot-triple junction interaction and oceanic plateau formation. *Journal Geophysical Research*, *104*(B4), 7539–7556. https://doi.org/10.1029/1999JB900002

Nakanishi, M., Tamaki, K., & Kobayashi, K. (1989). Mesozoic magnetic lineations and seafloor spreading history of the northwestern Pacific. *Journal Geophysical Research*, *94*(B11), 15,437–15,462. https://doi.org/10.1029/JB094iB11p15437

O'Connor, J. M., Hoernle, K., Müller, R. D., Morgan, J. P., Butterworth, N. P., Hauff, F., et al. (2015). Deformation-related volcanism in the Pacific Ocean linked to the Hawaiian-Emperor bend. *Nature Geosciences*, *8*(5), 393–397. https://doi.org/10.1038/ngeo2416

Ogg, J. G. (2012). Geomagnetic polarity time scale (Chapter 5). In F. M. Gradstein, J. G. Ogg, M. Schmitz, & G. Ogg (Eds.), *The Geologic Time Scale 2012*, (pp. 85–113). https://doi.org/10.1016/B978-0-444-59425-9.00005-6

O'Neill, C., Müller, R. D., & Steinberger, B. (2005). On the uncertainties in hot spot reconstructions and the significance of moving hot spot reference frames. *Geochemistry, Geophysics, Geosystems*, *6*, Q04003. https://doi.org/10.1029/2004GC000784

Pringle, M. S., & Dalrymple, G. B. (1993). Geochronological constraints on a possible hot spot origin for Hess Rise and the Wentworth Seamount Chain. In M. S. Pringle, W. W. Sager, W. V. Sliter, & S. Stein (Eds.), *The Mesozoic Pacific: Geology, Tectonics, and Volcanism*, *Am. Geophys. Union Geophys. Monogr* (Vol. 77, pp. 263–277). Washington, DC: American Geophysical Union.

Pringle, M. S., & Duncan, R. A. (1995). Radiometric ages of basaltic lavas recorded at Site 865, 866 and 869. In *Proceedings Ocean Drilling Program, Scientific Results* (Vol. 143, pp. 277–283). Washington: Americal Geophysical Union

Riisager, P., Hall, S., Antretter, M., & Zhao, X. (2003). Paleomagnetic paleolatitude of Early Cretaceous Ontong Java Plateau basalts: Implications for Pacific apparent and true polar wander. *Earth and Planetary Science Letters*, *208*(3-4), 235–252. https://doi.org/10.1016/S0012-821X(03)00046-3

Sager, W. W. (2005). What built Shatsky Rise, a mantle plume or ridge tectonics? In G. R. Foulger, J. H. Natland, D. C. Presnall, & D. L. Anderson (Eds.), *Plates, plumes, and paradigms*, *Geological Society of America Special Paper*, (Vol. 388, pp. 721–733). Boulder, Colorado: Geological Society of America. https://doi.org/10.1130/2005.2388(41)

Sager, W. W., Handschumacher, D. W., Hilde, T. W. C., & Bracey, D. R. (1988). Tectonic evolution of the northern Pacific plate and Pacific-Farallon-Izanagi triple junction in the Late Jurassic and Early Cretaceous (M21–M10). *Tectonophysics*, *155*(1-4), 345–364. https://doi.org/10.1016/0040-1951(88)90274-0

Sager, W. W., Kim, J., Klaus, A., Nakanishi, M., & Khankishieva, L. M. (1999). Bathymetry of Shatsky Rise, northwest Pacific Ocean: Implications for ocean plateau development at a triple junction. *Journal Geophysical Research*, *104*(B4), 7557–7576. https://doi.org/10.1029/1998JB900009

Sager, W. W., Pueringer, M., Carvallo, C., Ooga, M., Housen, B., & Tominaga, M. (2015). Paleomagnetism of igneous rocks from the Shatsky Rise: Implications for paleolatitude and oceanic plateau volcanism. In C. R. Neal, W. W. Sager, T. Sano, & E. Erba (Eds.), Special Paper 511 (8)*The origin, evolution, and environmental impact of oceanic large igneous provinces*, *Geological Society of America Special Paper*, (Vol. 511, pp. 147–171). Boulder, Colorado: Geological Society of America.

Sager, W. W., Sano, T., & Geldmacher, J. (2016). Formation and evolution of Shatsky Rise oceanic plateau: Insights from IODP Expedition 324 and recent geophysical cruises. *Earth Science Reviews*, *159*, 306–336. https://doi.org/10.1016/j.earscirev.2016.05.011

Sager, W. W., Zhang, J., Korenaga, J., Sano, T., Koppers, A. A. P., Widdowson, M., & Mahoney, J. J. (2013). An immense shield volcano within the Shatsky Rise oceanic plateau, northwest Pacific Ocean. *Nature Geosciences*, *6*, 976–981. https://doi.org/10.1038/ngeo1934

Sandwell, D. T., Müller, R. D., Smith, W. H. F., Garcia, E., & Francis, R. (2014). New global marine gravity model from CryoSat-2 and Jason-1 reveals buried tectonic structure. *Science*, *346*(6205), 65–67. https://doi.org/10.1126/science.1258213

Sayre, W. O. (1981). Preliminary report on the paleomagnetism of Aptian and Albian limestones and trachytes from the Mid-Pacific mountains and Hess rise. Deep Sea Drilling Project Leg 2. In *Initial Report, Deep Sea Drilling Project*, (Vol. 62, pp. 983–994). Washington, D.C: U.S. Government Printing Office.

Seton, M., Müller, R. D., Zahirovic, S., Gaina, C., Torsvik, T., Shephard, G., et al. (2012). Global continental and ocean basin reconstructions since 200 Ma. *Earth Science Reviews*, *113*(3-4), 212–270. https://doi.org/10.1016/j.earscirev.2012.03.002

Seton, M., Whittaker, J., Wessel, P., Müller, R. D., DeMets, C., Merkouriev, S., et al. (2014). Community infrastructure and repository for marine magnetic identifications. *Geochemistry, Geophysics, Geosystems*, *5*, 1629–1641. https://doi.org/10.1002/2013GC005176

Shephard, G. E., Matthews, K. J., Hosseini, K., & Domeier, M. (2017). On the consistency of seismically imaged lower mantle slabs. *Science Reports*, *7*(1), 10976. https://doi.org/10.1038/s41598-017-11039-w

Shephard, G. E., Müller, R. D., & Seton, M. (2013). The tectonic evolution of the Arctic since Pangea breakup: Integrating constraints from surface geology and geophysics with mantle structure. *Earth-Science Reviews*, *124*, 148–183. https://doi.org/10.1016/j.earscirev.2013.05.012

Sigloch, K., & Mihalynuk, M. G. (2013). Intra-oceanic subduction shaped the assembly of Cordilleran North America. *Nature*, *496*(7443), 50–56. https://doi.org/10.1038/nature12019

Sleep, N. H. (1997). Lateral flow and ponding of starting plume material. *Journal Geophysical Research*, *102*(B5), 10,001–10,012. https://doi.org/10.1029/97JB00551

Steinberger, B. (2000). Plumes in a convecting mantle: Models and observations for individual hotspots. *Journal Geophysical Research*, *105*(B5), 11,127–11,152. https://doi.org/10.1029/1999JB900398

Steinberger, B., & Gaina, C. (2007). Plate tectonic reconstructions predict part of Hawaiian hotspot track to be preserved in Bering Sea. *Geology*, *35*(5), 407–410. https://doi.org/10.1130/G23383A.1

Steinberger, B., & O'Connell, R. J. (1998). Advection of plumes in mantle flow: Implications for hotspot motion, mantle viscosity and plume distribution. *Geophysical Journal International*, *132*(2), 412–434. https://doi.org/10.1046/j.1365-246x.1998.00447.x

Steinberger, B., Sutherland, R., & O'Connell, R. J. (2004). Prediction of Emperor-Hawaii seamount locations from a revised model of global plate motion and mantle flow. *Nature*, *430*(6996), 167–173. https://doi.org/10.1038/nature02660. PMID:15241405

Steinberger, B., & Torsvik, T. H. (2008). Absolute plate motions and true polar wander in the absence of hotspot tracks. *Nature*, *452*(7187), 620–623. https://doi.org/10.1038/nature06824

Svensen, H. H., Torsvik, T. H., Callegaro, S., Augland, L., Heimdal, T., Jerram, D., et al. (2017). Gondwana LIPs: Plate reconstructions, volcanic basins and sill intrusions. In S. Sensarma, & B. C. Storey (Eds.), *Large igneous provinces from Gondwana and adjacent regions*, Geological Society London Special Publications (Vol. *463*, 24 pp.). Boulder, CO: Geological Society of America. https://doi.org/10.1144/SP463.7

Tarduno, J.A. & Bono, R. (2019). Hotspot and LLSVP wander. *Geophysical Research Abstracts* Vol. 21, EGU2019-3143, 2019 EGU General Assembly.

Tarduno, J. A., & Cottrell, R. D. (1997). Palaeomagnetic evidence for motion of the Hawaiian hotspot formation of the Emperor seamounts. *Earth and Planetary Science Letters*, *153*(3-4), 171–180. https://doi.org/10.1016/S0012-821X(97)00169-6

Tarduno, J. A., & Koppers, A. A. P. (2019). When hotspots move: The new view of mantle dynamics made possible by scientific ocean drilling. *Oceanography*, *32*(1), 150–152. https://doi.org/10.5670/oceanog.2019.137

Tauxe, L. (2005). Inclination flattening and the geocentric axial dipole hypothesis. *Earth and Planetary Science Letters*, *233*(3-4), 247–261. https://doi.org/10.1016/j.epsl.2005.01.027

Taylor, B. (2006). The single largest oceanic plateau: Ontong Java–Manihiki–Hikurangi. *Earth and Planetary Science Letters*, *241*(3-4), 372–380. https://doi.org/10.1016/j.epsl.2005.11.049

Tejada, M. L. G., Geldmacher, J., Hauff, F., Heaton, D., Koppers, A. A. P., Garbe-Schonberg, D., et al. (2016). Geochemistry and age of Shatsky, Hess, and Ojin Rise seamounts: Implications for a connection between the Shatsky and Hess Rises. *Geochimica et Cosmochimica Acta*, *185*, 302–327. https://doi.org/10.1016/j.gca.2016.04.006

Tominaga, M., Evans, H. F., & Iturrino, G. (2012). "Equator Crossing" of Shatsky Rise? New insights on Shatsky Rise tectonic motion from the downhole magnetic architecture of the uppermost lava sequences at Tamu Massif. *Geophysical Research Letters*, *39*, L21301. https://doi.org/10.1029/2012GL052967

Tominaga, M., Sager, W. W., & Channell, J. E. T. (2005). Paleomagnetism of the igneous section, Hole 1213B, Shatsky Rise. In T. J. Bralower, I. Premoli Silva, M. J. Malone, et al. (Eds.), *Proceedings of the Ocean Drilling Program, Scientific Results* (Vol. 198, 15 pp.). College Station, TX: Ocean Drilling Program. https://doi.org/10.2973/odp.proc.sr.198.113.2005

Torsvik, T. H., Amundsen, H., Hartz, E., Corfu, F., Kusznir, N., Gaina, C., et al. (2013). A Precambrian microcontinent in the Indian Ocean. *Nature Geoscience*, *6*(3), 223–227. https://doi.org/10.1038/ngeo1736

Torsvik, T. H., Amundsen, H. E. F., Trønnes, R. G., Doubrovine, P. V., Gaina, C., Kusznir, N., et al. (2015). Continental crust beneath southeast Iceland. *Proceedings of the National Academy of Sciences*, *112*(15), E1818–E1827. https://doi.org/10.1073/pnas.1423099112

Torsvik, T. H., & Cocks, L. R. M. (2013). GR focus review: Gondwana from top to base in space and time. *Gondwana Research*, *24*, 999–1030.

Torsvik, T. H., & Cocks, L. R. M. (2017). *Earth history and palaeogeography*, (Vol. 317). Cambridge: Cambridge University Press. https://doi.org/10.1017/9781316225523

Torsvik, T. H., Doubrovine, P. V., Steinberger, B., Gaina, C., Spakman, W., & Domeier, M. (2017). Pacific plate motion change caused the Hawaiian-Emperor Bend. *Nature Communications*, *8*(1), 15660. https://doi.org/10.1038/ncomms15660

Torsvik, T. H., Müller, R. D., Van der Voo, R., Steinberger, B., & Gaina, C. (2008). Global plate motion frames: Toward a unified model. *Review of Geophysics*, *46*, RG3004. https://doi.org/10.1029/2007RG000227

Torsvik, T. H., Rousse, S., Labails, C., & Smethurst, M. A. (2009). A new scheme for the opening of the South Atlantic Ocean and dissection of an Aptian Salt Basin. *Geophysical Journal International*, *177*(3), 1315–1333. https://doi.org/10.1111/j.1365-246X.2009.04137.x

Torsvik, T. H., Smethurst, M. A., Burke, K., & Steinberger, B. (2006). Large Igneous Provinces generated from the margins of the Large Low Velocity Provinces in the deep mantle. *Geophysical Journal International*, *167*, 1447–1460.

Torsvik, T. H., Steinberger, B., Ashwal, L. D., Doubrovine, P. V., & Trønnes, R. G. (2016). Earth evolution and dynamics—A tribute to Kevin Burke. *Canadian Journal Earth Sciences*, *53*(11), 1073–1087. https://doi.org/10.1139/cjes-2015-0228

Torsvik, T. H., Steinberger, B., Gurnis, M., & Gaina, C. (2010). Plate tectonics and net lithosphere rotation over the past 150 My. *Earth and Planetary Science Letters*, *291*(1-4), 106–112. https://doi.org/10.1016/j.epsl.2009.12.055

Torsvik, T. H., Van der Voo, R., Preeden, U., Mac Niocaill, C., Steinberger, B., Doubrovine, P. V., et al. (2012). Phanerozoic polar wander, paleogeography and dynamics. *Earth Science Reviews*, *114*(3-4), 325–368. https://doi.org/10.1016/j.earscirev.2012.06.007

van Der Meer, D. G., Spakman, W., Van Hinsbergen, D. J., Amaru, M. L., & Torsvik, T. H. (2010). Toward absolute plate motions constrained by lower-mantle slab remnants. *Nature Geoscience*, *3*(1), 36–40. https://doi.org/10.1038/ngeo708

van der Meer, D. G., Torsvik, T. H., Spakman, W., van Hinsbergen, D. J. J., & Amaru, M. L. (2012). Intra-Panthalassa Ocean subduction zones revealed by fossil arcs and mantle structure. *Nature Geoscience*, *5*(3), 215–219. https://doi.org/10.1038/ngeo1401

van der Meer, D. G., van Hinsbergen, D. J. J., & Spakman, W. (2017). The Atlas of the underworld: a catalog of slab remnants in the mantle imaged by seismic tomography, and their geological interpretation. *Tectonophysics*, *723*, 309–448. https://doi.org/10.1016/j.tecto.2017.10.004

Wallick, B. P., & Steiner, M. B. (1992). Paleomagnetic and rock magnetic properties of Jurassic Quiet Zone basalts, Hole 801C. In *Proceedings of the Ocean Drilling Program, Scientific Results* (Vol. 129, pp. 455–470). College Station, Texas: Ocean Drilling Program.

Wang, S., Yua, H., Zhang, Q., & Zhao, Y. (2018). Absolute plate motions relative to deep mantle plumes. *Earth and Planetary Science Letters*, *490*, 88–99. https://doi.org/10.1016/j.epsl.2018.03.021

Wessel, P., & Kroenke, L. W. (2008). Pacific absolute plate motion since 145 Ma: An assessment of the fixed hot spot hypothesis. *Journal Geophysical Research*, *113*, B06101. https://doi.org/10.1029/2007JB005499

Winterer, E. L., & Sager, W. W. (1995). Synthesis of drilling results from the Mid-Pacific Mountains: Regional context and implications. In *Proceedings of the Ocean Drilling Program, scientific results*, (Vol. 143, pp. 497–535). College Station, Texas: Ocean Drilling Program.

Wright, N. M., Müller, R. D., Seton, M., & Williams, S. E. (2015). Revision of Paleogene plate motions in the Pacific and implications for the Hawaiian-Emperor bend. *Geology*, *43*(5), 455–458. https://doi.org/10.1130/G36303.1

Wright, N. M., Seton, M., Williams, S. E., & Müller, R. D. (2016). The Late Cretaceous to recent tectonic history of the Pacific Ocean basin. *Earth-Science Reviews*, *154*, 138–173. https://doi.org/10.1016/j.earscirev.2015.11.015